Journal of the Korean Ceramic Society
Vol. 44, No. 12, pp. 660~682, 2007.

Defect Structure, Nonstoichiometry and Nonstoichiometry Relaxation of Complex Oxides

Han-Ill Yoo†

Department of Materials Science and Engineering, Seoul National University, Seoul 151-744, Korea
(Received November 13, 2007; Accepted December 3, 2007)

ABSTRACT

An SOFC consists of all ceramic complex oxides each with different electrochemical-property requirements. These requirements, in principle, can be made met to a great extent by controlling or tailoring the defect structure of the oxide. This paper reviews the defect structure, nonstoichiometry as a measure of the total defect concentration, and the defect relaxation kinetics of complex oxides that are currently involved in a variety of growing applications today.

Key words **: *Defect structure, Nonstoichiometry, Nonstoichiometry Relaxation, Complex Oxides, SOFC***

1. Introduction

Crystalline oxide materials have long garnered a vast range of technological interest in optical, electrical, magnetic, thermal, chemical, and electrochemical applications. They often comprise no less than three components in at least than three sublattices, and tend to be even more complex in terms of the number of components and sublattices. The simplest examples may be those with a perovskite structure (ABO_3) or a spinel structure (AB_2O_4).

For all applications of complex oxides, knowledge and control of their defect structure is essential to endow them with their necessary functions as well as to design and/or optimize the processing route of relevant devices. By the defect structure, we mean the types, concentrations and spatial distributions of mainly point defects. For the best electrochemical performance of an SOFC electrode oxide, for example, the oxide should be defect-chemically processed to have as high an oxide ionic conductivity as possible while suppressing cationic mobility as much as possible, in addition to a sufficiently high level of electronic conductivity. Another example may be positive temperature coefficient resistors (PTCR) based on $BaTiO_3$: the interior of $BaTiO_3$ grains should be made n-type semiconducting by doping donor impurities and the grain boundaries electrically insulating by oxidation.[1] The thickness of a grain boundary insulation layer should be carefully controlled for optimum PTCR performance by appropriately adjusting the magnitude and distribution of oxygen nonstoichiometry during cooling after sintering. A further example may be $BaTiO_3$-based multilayer ceramic capacitors (MLCC) employing base metal electrodes (e.g., Ni): it should be sintered in a reducing atmosphere to avoid oxidation of the base metal while suppressing the reduction-generated electrons and oxygen vacancies in order to retard the insulation-resistance degradation while the devices are in service. In a sense, control or tailoring of the defect structure is similar to blowing the soul into the body, an art of making oxides functionally alive.

The basic principle behind the control or tailoring of the defect structure is that point defects are thermodynamically stable and hence, their concentrations, as thermodynamic equilibrium properties, can be uniquely determined by the independent thermodynamic variables, namely, temperature, pressure and compositions or their conjugate chemical potentials of the system. This is a basic thermodynamic postulate, that may even be called the "-1^{st} law of thermodynamics." Thus, by adjusting the temporal and spatial distribution of these thermodynamic variables, one can, in principle, adjust the temporal and spatial distribution of defects.

Defects are not a conserved entity: they can be annihilated or generated normally via solid state diffusion from or to repeatable growth sites such as surfaces, grain boundaries and dislocations. Solid-state diffusion is a time and energy-consuming process. One may, thus, kinetically cheat the defect structure by adjusting the time rate of the thermodynamic variables. The latter is often taken advantage of in actual processes to freeze-in a non-equilibrium defect structure for the purpose of controlling the properties.

In this article, we will consider the thermodynamic and kinetic aspects of the defect structure in complex oxides with application in mind. As a prototype of complex oxides, this paper specifically refers to $BaTiO_3$ among others because, to the best of the author's knowledge, the experimental data related to $BaTiO_3$ have been extensively and consistently documented. This is not intended as an exhaustive literature review, but propose instead to convey the

†Corresponding author : Han-Ill Yoo
E-mail : hiyoo@snu.ac.kr
Tel : +82-2-880-7163 Fax : +82-2-884-1413

thermodynamic and kinetic behavior of the defect structure in complex oxides. Even if $BaTiO_3$ is referred to exclusively here, the information can easily apply to other complex oxide systems with minor modifications.

The configuration of the article will be as follows. In Section 2, we will summarize how to calculate the equilibrium defect structure of the prototype complex oxide as a function of independent thermodynamic variables. Once a batch composition in terms of the component oxides, say BaO and TiO_2 is formulated, the only possible control of the defect structure during processing is normally via the exchange of the volatile component, for instance oxygen during heat treatment. This adjusts the oxygen nonstoichiometry that eventually governs the concentration of charge carriers, oxygen vacancies, electrons and holes that often drastically affect the performance of the oxide-based devices. In Section 3, we will see how oxygen nonstoichiometry, as a measure of the concentration of electronic carriers, varies with the thermodynamic variables and its defect-chemical implications. Adjustment of oxygen nonstoichiometry can be achieved to a great extent by chemical diffusion processes under an oxygen potential gradient imposed during actual processing of an oxide or related devices. Section 4 examines how oxygen nonstoichiometry relaxes in an oxygen potential gradient in connection with the defect structure.

2. Defect Structure

The logical framework to calculate defect structure of a complex oxide has earlier been laid by Wagner and Schmalzried.[2,3] The basic idea behind is to solve the simultaneous equations involving concentrations of the structure elements, be they regular or irregular, that are based on a series of constraints of internal (thermal) equilibria, external (particle exchange) equilibria, crystal structure preservation, charge neutrality, and mass conservation (when doped). The internal equilibria are determined by temperature only under ambient pressure (P = 1 atm), but the external ones are determined by the independent activities of the chemical components in addition to the temperature. We will, thus, end up with a concentration as a function of the intensive thermodynamic variables of the given system, viz., temperature and independent activities of the components. We will apply this idea to calculate the defect structures of $BaTiO_3$ for pure, acceptor-doped and donor-doped cases, respectively.

2.1. Pure case

Let us first consider pure $BaTiO_3$. For a ternary system, there are two composition variables, e.g., mole fractions of Ti and O. When there are three sublattices, however, it is more convenient to choose the molecular ratio of the component oxides, BaO and TiO_2 and the equivalent ratio of the non-metallic components to the metallic components[3,4] or

$$1+\eta \equiv \frac{[Ti]_t}{[Ba]_t}; \quad 1-\frac{1}{3}\delta \equiv \frac{2[O]_t}{2[Ba]_t+4[Ti]_t} \tag{2.1}$$

where $[\ ]_t$ represents the total concentration of the component therein. The lattice molecule may then be represented more appropriately as

$$BaTi_{1+\eta}O_{3+2\eta-\delta} \tag{2.2}$$

where η is called the deviation from the molecularity($\eta=0$) or nonmolecularity, and δ the deviation from the stoichiometry($\delta=0$) or nonstoichiometry of the compound. Any thermodynamic equilibrium property of the system is given as a function of independent thermodynamic variables of the system under the atmospheric pressure, temperature (T), the activity of a component oxide, say, TiO_2 (a_{TiO_2}) and the activity of oxygen (a_{O_2}) or equivalently by their conjugate variables η and δ, considering the Gibbs-Duhem equation for the system.

One may start by conjecturing the possible defects of the oxide from its structural and energetic considerations. For the system of perovskite structure, the interstitial defects may be ruled out and hence, the structure elements the concentrations of which we want to know may be the irregular structure elements: V''_{Ba}, V''''_{Ti}, $V^{\cdot\cdot}_O$, e', $h^{\cdot}$; in addition to the regular structure elements: Ba^x_{Ba}, Ti^x_{Ti}, O^x_O; in terms of the Kröger-Vink notation.

Letting [S] denote the concentration (in number/cm^3) of the structure element S ($[e']\equiv n$, $[h^{\cdot}]\equiv p$), one may formulate all the constraints assuming an ideal dilute solution behavior of defects as:

(i) Internal equilibria:

$$0 = e' + h^{\cdot} \quad ; \quad K_i = np \tag{2.3}$$

$$0 = V''_{Ba} + V''''_{Ti} + 3V^{\cdot\cdot}_O \quad ; \quad K_s = [V''_{Ba}][V''''_{Ti}][V^{\cdot\cdot}_O]^3 \tag{2.4}$$

(ii) External equilibria:

$$O^x_O = V^{\cdot\cdot}_O + 2e' + \frac{1}{2}O_2(g) \quad ; \quad K_{Re} = [V^{\cdot\cdot}_O]n^2 a_{O_2}^{1/2} \tag{2.5}$$

$$TiO_2 = Ti^x_{Ti} + 2O^x_O + V''_{Ba} + V^{\cdot\cdot}_O \quad ; \quad K_T = \frac{[V''_{Ba}][V^{\cdot\cdot}_O]}{a_{TiO_2}} \tag{2.6}$$

(iii) Charge neutrality:

$$n + 2[V''_{Ba}] + 4[V''''_{Ti}] = p + 2[V^{\cdot\cdot}_O] \tag{2.7}$$

(iii) Structure preservation:

$$1\beta = [Ba^x_{Ba}] + [V''_{Ba}] \tag{2.8}$$

$$1\beta = [Ti^x_{Ti}] + [V''''_{Ti}] \tag{2.9}$$

$$3\beta = [O^x_O] + [V^{\cdot\cdot}_O] \tag{2.10}$$

with $\beta = N_A/V_m$ where N_A and V_m being the Avogadro number and the molar volume of the system, respectively.

Here, the mass-action law constants are denoted as K_j(j = Re, T, S, i) which may be represented as

$$K_j = K_j^o \exp\left(-\frac{\Delta H_j}{kT}\right) \tag{2.11}$$

where K_j^o is the pre-exponential factor and ΔH_j the enthalpy change of the associated reaction j.

Table 1. Matrix of Majority Disorder Types in the Systems of $BaTiO_3$. The Top Left Rectangle Demarcated by Thick Solid Lines is for the Pure Case; this Rectangle Plus the Rightmost Column for the Acceptor-doped Case; the Rectangle Plus the Bottommost Row for the Donor-doped Case. A Pair of Signs Out of +,0,− at each Element are for η and δ: e.g., (+,0) is for η>0 and (δ≈0)

+ \ −	n	$2[V''_{Ba}]$	$4[V''''_{Ti}]$	$[A'_C]$
p	n=p (0 ; 0)	$p=2[V''_{Ba}]$ (+ ; −)	$p=4[V''''_{Ti}]$ (− ; −)	$p=[A'_C]$ (+ ; −)
$2[V^{\cdot\cdot}_O]$	$2[V^{\cdot\cdot}_O]=n$ (0 ; +)	$[V^{\cdot\cdot}_O]=[V''_{Ba}]$ (+ ; 0)	$[V^{\cdot\cdot}_O]=2[V''''_{Ti}]$ (− ; 0)	$2[V^{\cdot\cdot}_O]=[A'_C]$ (+ ; 0)
$[D^{\cdot}_C]$	$[D^{\cdot}_C]=n$ (− ; +)	$[D^{\cdot}_C]=2[V''_{Ba}]$ (− ; 0)	$[D^{\cdot}_C]=4[V''''_{Ti}]$ (− ; 0)	

It is noted that there are exactly 8 equations (Eqs. 2.3-2.10) for 8 unknowns (V''_{Ba}, V''''_{Ti}, $V^{\cdot\cdot}_O$, e', h$^{\cdot}$, Ba^x_{Ba}, Ti^x_{Ti}, O^x_O). As the concentrations of irregular structure elements are normally much smaller than those of regular structure elements, Eqs. 2.8 to 2.10 turn trivial (i.e., $[Ba^x_{Ba}]\approx[Ti^x_{Ti}]\approx[O^x_O]/3\approx 1\beta$) and hence, one may delete the regular structure elements from the list of the unknowns. Then, note that when one started with "q" irregular structure elements in a c-component system, there would always be (c-1) external equilibrium conditions and (q-c) internal equilibrium conditions and 1 charge neutrality condition to determine all those n unknowns completely.

In principle, one can solve this set of equations simultaneously for each defect concentration in terms of $K_j(T)$, a_{TiO_2}, and a_{O_2} or

$$[S]=f(K_j, a_{TiO_2}, a_{O_2}) \tag{2.12}$$

However, it is usually prohibitively messy: the culprit is that the algebraic structure of the charge neutrality condition, Eq. 2.7, is different from the rest, Eqs. 2.3-2.6. The normal practice is, thus, to approximate the charge neutrality condition by a limiting condition or in terms of an oppositely charged pair of disorders in the majority (Brouwer approximation[4]) depending on the thermodynamic conditions.

All the possible types of majority disorder may be distinguished by constructing a matrix with the positively charged disorders as row and the negatively charged ones as column (vice versa, of course) as shown in Table 1.[3,4] In the case of pure $BaTiO_3$, there can be 2×3 elements or 6 possible majority disorder types.

By using the limiting charge neutrality condition in terms of a majority disorder pair in Table 1, one can now solve with no algebraic awkwardness at all each defect concentration in the form of [3,4]

$$[S]=a^m_{O_2}a^n_{TiO_2}\prod_j K^s_j \tag{2.13}$$

The numerical values for the exponents "m" and "n" (not to be confused with the electron concentration in Eq. 2.3) in each majority disorder regime are listed (in the form of m ; n at each element) in Table 2.

In order to construct a complete picture of defect structure against the thermodynamic variables particularly a_{TiO_2} and a_{O_2} over their entire ranges, one should combine these piecewise solutions, Eq. 2.13 in appropriate order. For this purpose, one should first know the distribution of the majority disorder types in the thermodynamic configuration space of $\log a_{O_2}$ vs. $\log a_{TiO_2}$ at fixed temperature. A simple method to find the configuration of the majority disorder types goes as follows[3,4]:

For the present system, Eq. 2.2, the nonmolecularity may

Table 2. Numerical Values for m and n Such that $[S]=a^m_{O_2}a^n_{TiO_2}\prod_j K^s_j$ in Each Majority Disorder Regime of Table 1

	n=p	$p=4[V''''_{Ti}]$	$2[V''''_{Ti}]=[V^{\cdot\cdot}_O]$	$2[V^{\cdot\cdot}_O]=n$	$[V^{\cdot\cdot}_O]=[V''_{Ba}]$	$2[V''_{Ba}]=p$
n	0 ; 0	−1/5 ; 1/5	−1/4 ; 1/6	−1/6 ; 0	−1/4 ; −1/4	−1/6 ; −1/3
p	0 ; 0	1/5 ; −1/5	1/4 ; −1/6	1/6 ; 0	1/4 ; 1/4	1/6 ; 1/3
$[V''_{Ba}]$	1/2 ; 1	1/10 ; 7/5	0 ; 4/3	1/6 ; 1	0 ; 1/2	1/6 ; 1/3
$[V''''_{Ti}]$	1 ; −1	1/5 ; −1/5	0 ; −1/3	1/3 ; −1	0 ; −2	1/3 ; −7/3
$[V^{\cdot\cdot}_O]$	−1/2 ; 0	−1/10 ; −2/5	0 ; −1/3	−1/6 ; 0	0 ; 1/2	−1/6 ; 2/3
$[A'_C]$	− ; −	− ; −	− ; -	0 ; 0	− ; −	− ; −
$[A^x_C]$	− ; −	− ; -	− ; −	1/6 ; 0	− ; −	− ; −

	$p=[A'_C]$	$2[V^{\cdot\cdot}_O]=[A'_C]$		$[D^{\cdot}_C]=4[V''''_{Ti}]$	$[D^{\cdot}_C]=2[V''_{Ba}]$	$n=[D^{\cdot}_C]$
		$[A'_C]\cong[A]_t$	$[A^x_C]\cong[A]_t$			
n	0 ; 0	−1/4 ; 0	−1/6 ; 0	−1/4 ; 1/4	−1/4 ; −1/2	0 ; 0
p	0 ; 0	1/4 ; 0	1/6 ; 0	1/4 ; −1/4	1/4 ; 1/2	0 ; 0
$[V''_{Ba}]$	1/2 ; 1	0 ; 1	1/6 ; 1	0 ; 3/2	0 ; 0	1/2 ; 1
$[V''''_{Ti}]$	1 ; −1	0 ; −1	1/3 ; −1	0 ; 0	0 ; −3	1 ; −1
$[V^{\cdot\cdot}_O]$	−1/2 ; 0	0 ; 0	−1/6 ; 0	0 ; −1/2	0 ; 1	−1/2 ; 0
$[A'_C]$	0 ; 0	0 ; 0	−1/6 ; 0			
$[A^x_C]$	0 ; 0	1/4 ; 0	0 ; 0			

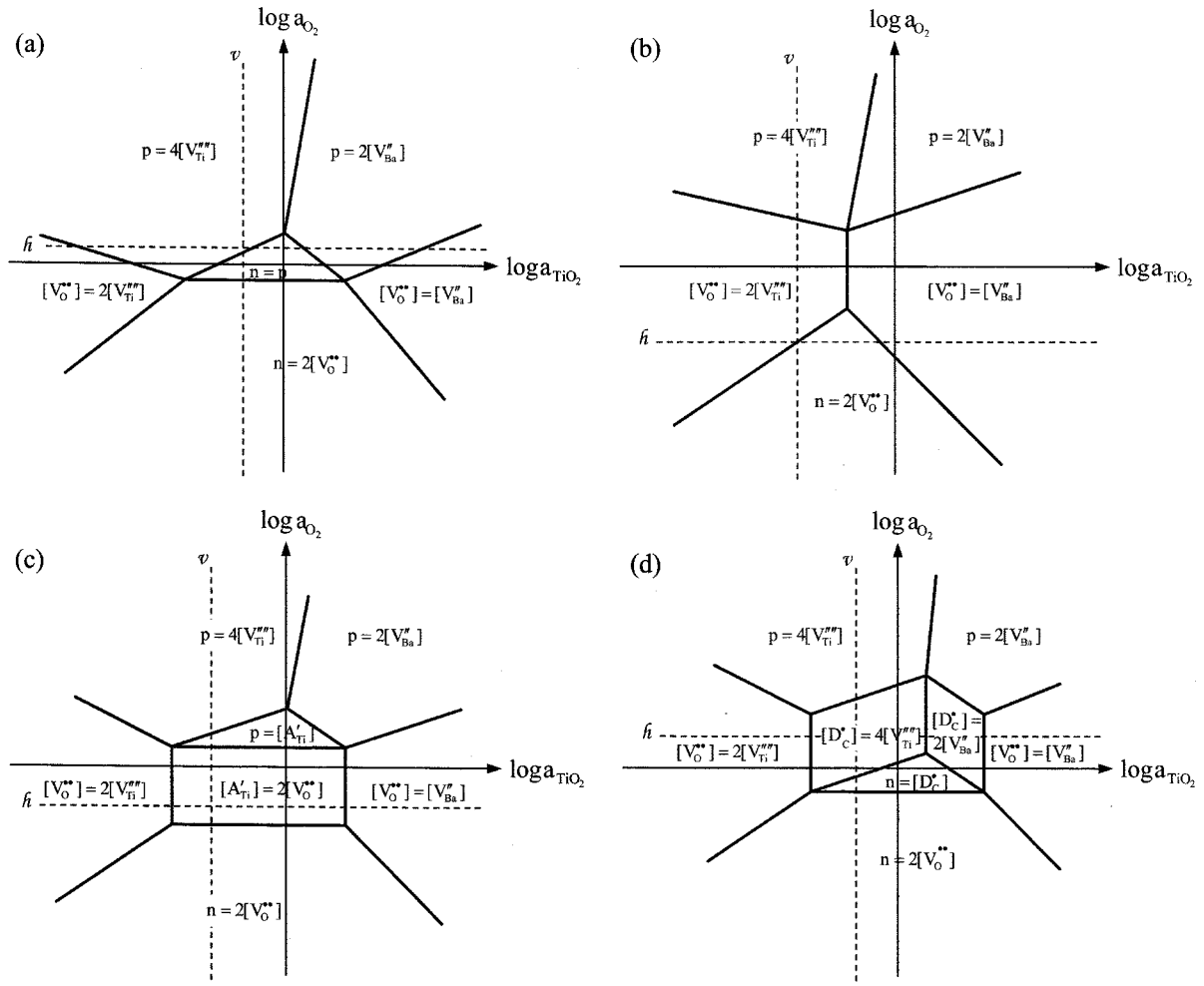

Fig. 2.1. Configuration of the majority disorder types on a plane of log a_{O_2} vs. log $aTiO_2$ at fixed temperature: (a) $K_i^{1/2} >> K_s^{1/5}$, $[A'_C]$,$[D_C^{\bullet}]$;(b) $K_s^{1/5} >> K_i^{1/2}$,$[A'_C]$,$[D_C^{\bullet}]$;(c)$[A'_C] >> K_i^{1/2}$,$K_s^{1/5}$,$[D_C^{\bullet}]$; (d) $[D_C^{\bullet}] >> K_i^{1/2}$,$K_s^{1/5}$,$[A'_C]$.

be represented in terms of irregular structure elements, due to Eqs. 2.1 and 2.8-2.10 as

$$\beta\eta \approx [V''_{Ba}] - [V'''_{Ti}] \tag{2.14}$$

as normally $[S]/\beta << 1$ if S is irregular. The nonstoichiometry, on the other hand, may be written as

$$\beta\delta \approx [V_O^{\bullet\bullet}] - [V''_{Ba}] - 2[V'''_{Ti}] = \frac{1}{2}(n-p) \tag{2.15}$$

for the same reason. The second equality is due to the charge neutrality condition, Eq. 2.7.

For each of the majority disorder types in Table 1, one can then determine by using Eqs. 2.14 and 2.15 whether η and δ are respectively larger than 0 (denoted as +), close to 0 (denoted as 0) or smaller than 0 (denoted as –). The results, pairs out of –,0 and + are given in the form of, e.g., (– ; 0) to each element in Table 1 where the first symbol is for η and the second for δ. In this identification, one should be aware that for the majority disorder type for which η can be both + and – as, e.g., for $n \approx p$ or $n \approx 2[V_O^{\bullet\bullet}]$, one may set $\eta \approx 0$.

There can be three regions along the axis of log a_{O_2}: $\delta > 0$ (oxygen deficit); ≈ 0 (near stoichiometry); < 0 (oxygen excess) with increasing a_{O_2}. Also three regions along the axis of log a_{TiO_2}: $\eta < 0$ (TiO_2-deficit); ≈ 0 (near molecularity); > 0 (TiO_2-excess) with increasing a_{TiO_2}. The configuration plane may, thus, be divided into 9 regions. One can then assign each majority disorder type to the region corresponding to its sign combination for (η ; δ) in Table 1. It happens quite often that multiple types fall in one region usually as the number of majority disorder types increase over 9. Again old wisdoms[5] help one not to get lost in finding the appropriate sequence of the majority disorder types. They are:

Rule 1. Near molecularity and stoichiometry region (0 ; 0): It is to be occupied by an intrinsic majority disorder type, either electronic or ionic disorder pair depending on which is energetically more favorable. In the present pure case, it depends on whether $K_i^{1/2} > K_s^{1/5}$ or $K_i^{1/2} < K_s^{1/5}$. Consequently intrinsic electronic and ionic disorder pairs normally do not fall congruently.

Rule 2. Other regions: The sequence in a given region outside the region (0 ; 0) is to be determined by the continuity principle, that is, any two neighboring regimes of majority disorder should have one defect of the defect pairs in common.

Rule 3. Majority disorder regime boundaries: Once the majority disorder types are located sequentially in the configuration plane of log a_{O_2} vs. log a_{TiO_2}, the two neighboring regimes of majority disorder meet in line when one defect of the two pairs is in common and otherwise at point. In the 3-dimensional space of log a_{O_2}-log a_{TiO_2}-1/T, the former would be a plane and the latter a line.

We may call these the allocation rules. By applying these rules, one can construct the configuration planes as shown in Fig. 2.1 (a) and (b) for the case of $K_i^{1/2} > K_s^{1/5}$ and $K_i^{1/2} < K_s^{1/5}$, respectively. Up to now, however, there has appeared no experimental evidence for $BaTiO_3$ which may even hint a possibility of $n \approx p$ being the majority disorder under any thermodynamic condition.

2.2. Acceptor-doped case

Next we will consider $BaTiO_3$ doped with fixed amount (x) of acceptor impurities A on, e.g., cation sites (generically denoted as A_C'). Specifically, they are assumed to be trivalent substituting Ti or A_{Ti}', e.g., Al_{Ti}'. The lattice molecule may then be written as

$$BaTi_{1-x+\eta}A_xO_{3-x/2+2\eta-\delta} \tag{2.16}$$

As one more defect species A_{Ti}' is added, one needs one more constraint in addition to those for the pure case: that is mass conservation or

$$[A_{Ti}'] = \beta x \tag{2.17}$$

The charge neutrality condition Eq. 2.7 and the site conservation conditions Eq. 2.9 should be accordingly modified, respectively, as

$$n + 2[V_{Ba}''] + 4[V_{Ti}''''] + [A_{Ti}'] = p + 2[V_O^{\cdot\cdot}] \tag{2.18}$$

$$1\beta = [Ti_{Ti}^x] + [V_{Ti}''''] + [A_{Ti}'] \tag{2.19}$$

In addition, while the nonmolecularity is still the same as Eq. 2.14, the nonstoichiometry should be modified due to Eq. 2.1 as

$$\beta\delta \approx [V_O^{\cdot\cdot}] - [V_{Ba}''] - 2[V_{Ti}''''] - \frac{1}{2}[A_{Ti}'] = \frac{1}{2}(n-p) \tag{2.20}$$

From Eq. 2.18 or from the matrix in Table 1, one can immediately distinguish 2×4 limiting conditions or 8 possible majority disorder types, but one should note that any intrinsic disorder type, n=p in the present case, cannot occupy the near molecularity-stoichiometry region (0 ; 0), because obviously $[A_{Ti}'] >> K_i^{1/2}$, $K_s^{1/5}$ or it would otherwise not be extrinsic due to the doped acceptors.

Again following Rules 1-3, one can construct the configuration plane of the majority disorder types as in Fig. 2.1(c) and in each regime, the values for the exponent m and n of Eq. 2.13 are given in Table 2.

2.3. Donor-doped case

Let us assume that our $BaTiO_3$ is now doped with a fixed amount (y) of donor impurities D on, e.g., the cation sites ($D_C^{\cdot}$). They are again assumed to be fixed-valent, but this time occupying Ba-site instead, or $D_{Ba}^{\cdot}$, e.g., $La_{Ba}^{\cdot}$. Then, the lattice molecule may be represented as

$$Ba_{1-y}D_yTi_{1+\eta}O_{3+y/2+2\eta-\delta} \tag{2.21}$$

As one more unknown $[D_{Ba}^{\cdot}]$ is added similarly to the acceptor-doped case, one mass-conservation equation for the dopant is added to Eqs. 2.3-2.6 as

$$[D_{Ba}^{\cdot}] = \beta y \tag{2.22}$$

In addition, the charge neutrality and site conservation conditions, Eqs. 2.7 and 2.8 are modified, respectively, to

$$n + 2[V_{Ba}''] + 4[V_{Ti}''''] = p + 2[V_O^{\cdot\cdot}] + [D_{Ba}^{\cdot}] \tag{2.23}$$

$$1\beta = [Ba_{Ba}^x] + [V_{Ba}''] + [D_{Ba}^{\cdot}] \tag{2.24}$$

The nonstoichiometry subsequently takes the form

$$\beta\delta \approx \frac{1}{2}(n-p) = [V_O^{\cdot\cdot}] - [V_{Ba}''] - 2[V_{Ti}''''] + \frac{1}{2}[D_{Ba}^{\cdot}] \tag{2.25}$$

while the nonmolecularity still remains the same as Eq. 2.14.

From Eq. 2.23 or Table 1, one can distinguish 3×3 possible limiting conditions or possible majority disorder types. But, again the intrinsic disorder type n=p is ruled out from the near molecularity-stoichiometry region (0 ; 0) in the configuration plane and hence, one is left with 8 majority disorder types. The configuration map of the majority disorder types can be constructed following Rules 1-3 as in Fig. 2.1(d). The reader may wish to check from the maps in Fig. 2.1 how those rules are working.

2.4. Two-dimensional representations of defect concentrations

Eq. 2.13 is basically a four dimensional representation (under a fixed total pressure) of defect structure, that is not so easy to visualize with ordinary vision. Normal practice is, thus, to represent in two dimensions: log [S] vs. log a_{TiO_2}(at fixed a_{O_2} and T), log[S] vs. log a_{O_2}(at fixed a_{TiO_2} and T), or log[S] vs. 1/T (at fixed a_{TiO_2} and a_{O_2}).

By combining the piecewise solutions, Eq. 2.13 with m and n values as given in Table 2 in accord with the configuration of the majority disorder types in Fig. 2.1, one can easily draw log [S] vs. log a_{TiO_2}(at fixed T and a_{O_2}) or vs. log a_{O_2} (at fixed a_{TiO_2} and T). The cross section along a horizontal dotted line in each of Fig. 2.1(a)-(d) (designated as "*h*"), for example, is shown in Fig. 2.2(a)-(d), which are nothing but log [S] vs. log a_{TiO_2}(at fixed T and a_{O_2}). Similarly, log [S] vs. log a_{O_2}(at given T and a_{TiO_2}) are shown in Fig. 2.3(a)-(d) which are the cross sections along the vertical dotted lines denoted as "*v*" in Fig. 2.1(a)-(d), respectively.

The reader is reminded that the representations, Figs. 2.2 and 2.3, are for the systems in equilibrium internally (Eqs. 2.3 and 2.4) as well as externally (Eqs. 2.5 and 2.6). In many cases, however, the external equilibria are often suspected for kinetic reasons. For $BaTiO_3$ and the like, for example,

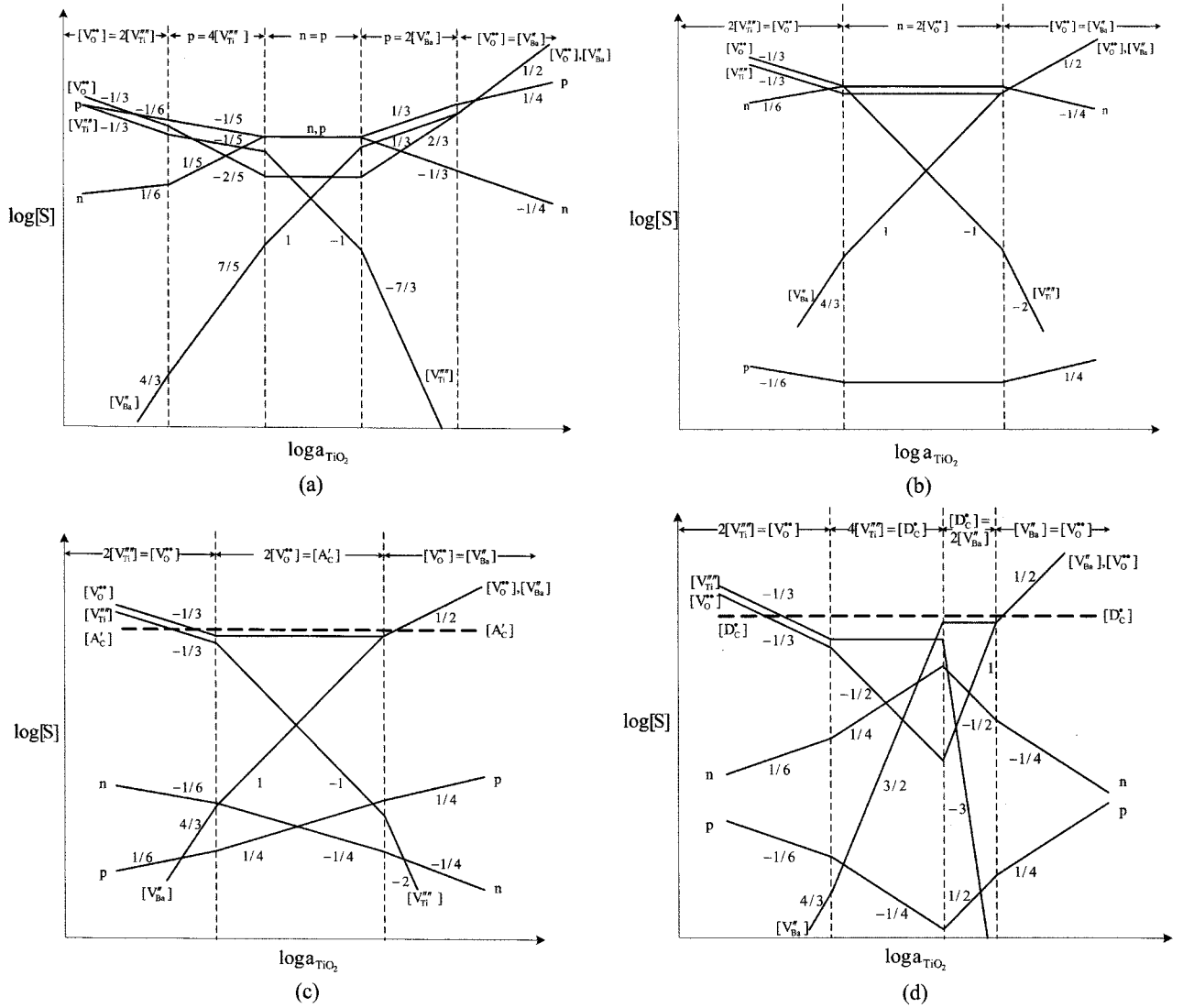

Fig. 2.2. Log [S] vs. log a_{TiO_2}, (a)-(d) corresponding to the horizontal dotted lines designated as "*h*" (fixed a_{O_2}) in Fig. 2.1(a)-(d), respectively.

chemical diffusion of oxygen is normally much faster than the metallic components and hence, while oxygen exchange equilibrium, Eq. 2.5, can be readily achieved, the metallic component exchange equilibrium, Eq. 2.6, can often be hardly achieved. If it is the case, a_{TiO_2} may not be held fixed while a_{O_2} varies. The extreme situation may be the case in which the system is closed with respect to the metallic components exchange so that the nonmolecularity η, instead of a_{TiO_2}, remains fixed by the initial batch composition across the entire range of log a_{O_2}. Depending largely on temperature, this situation may be more realistic than the complete thermodynamic equilibrium. One, thus, often needs to know how defect structure varies against a_{O_2} while η, instead of a_{TiO_2}, is held constant. Old wisdom[6] has already considered this problem. We will now transform log [S] vs. log a_{O_2} at fixed a_{TiO_2} in Fig. 2.3 to those at fixed η to see how they appear.

To make the situation simpler, let us assume that the initial batch composition, whether doped or not, is with a_{TiO_2}-deficit ($\eta<0$) such that

$$-\beta\eta \approx [V'''']_{Ti} >> [V''_{Ba}] \tag{2.26}$$

Then, one can immediately dictate the variation of -η versus a_{O_2} at fixed a_{TiO_2} by following the variation of $[V'''']_{Ti}$ in Fig. 2.3(a)-(d). It is noted there that even if a_{TiO_2} is held fixed, the nonmolecularity is changing with oxygen activity, meaning that material has to be exchanged with the surrounding for keeping the system in the external equilibrium.

In each of the majority disorder regimes, one can obtain from Eq. 2.13 for $[S]=[V'''']_{Ti} \approx -\beta\eta$,

$$a_{TiO_2}=a_{O_2}^{-m/n}(-\beta\eta)^{1/n}\prod_j K_j^{-s/n} \tag{2.27}$$

Each defect concentration in Eq. 2.13 can then be transformed, by replacing a_{TiO_2} with Eq. 2.27, into a form

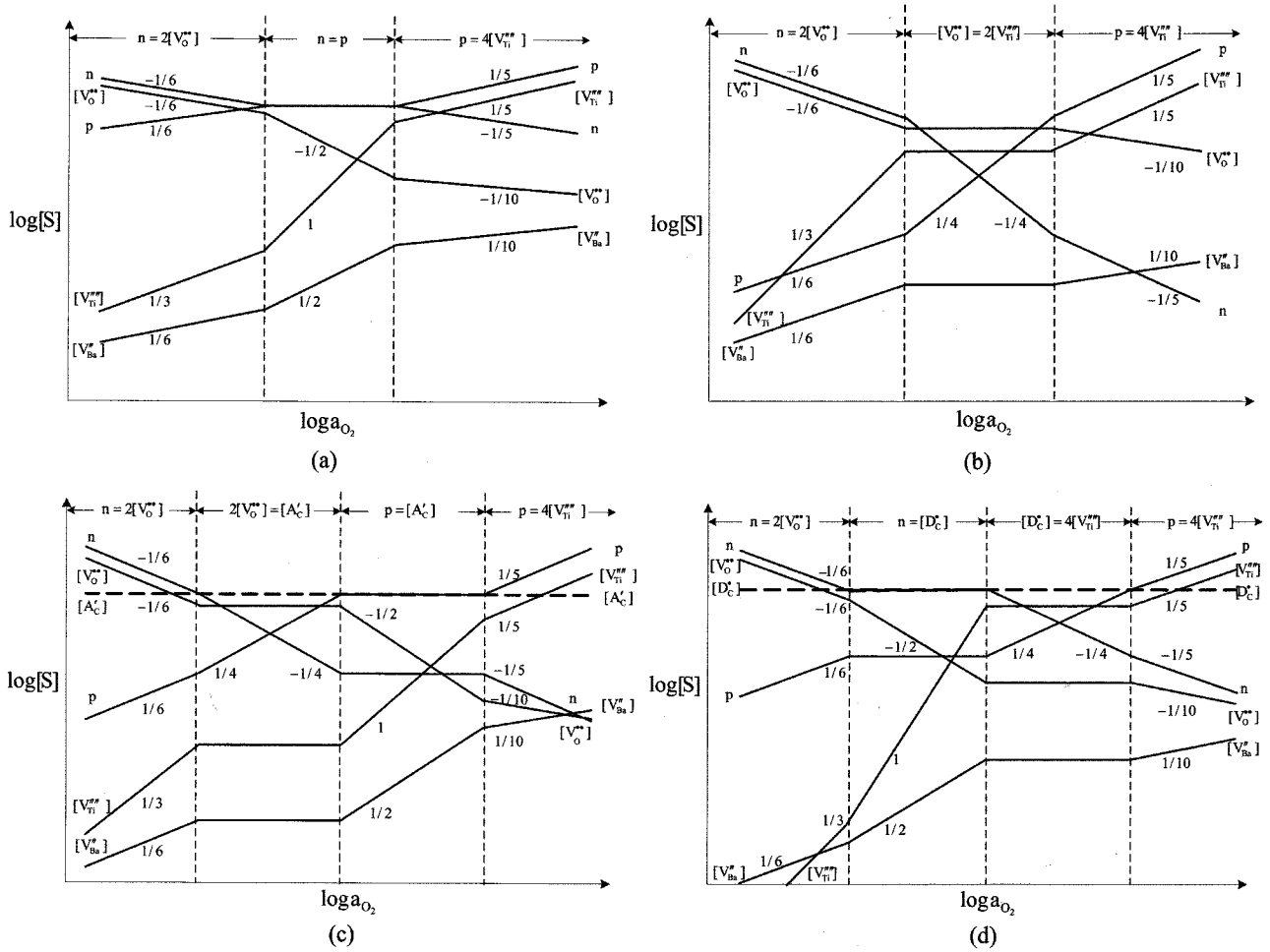

Fig. 2.3. Log [S] vs. log a_{O_2}, (a)-(d) corresponding to the vertical dotted lines designated as "v" (fixed a_{TiO_2}) in Fig. 2.1(a)-(d), respectively.

$$[S]=a_{O_2}^{p}(-\beta\eta)^{q}\prod_j K_j^{r} \quad \text{for } S\neq V_{Ti}'''' \tag{2.28}$$

By combining these piecewise solutions in accord with the appropriate sequence of the majority disorder types, in principle, one can transform Fig. 2.3 to those for fixed η. The sequence of the majority disorder types for fixed η will remain the same as that for fixed a_{TiO_2} due to Le Châtlier's principle,

$$\left(\frac{\partial(-\beta\eta)}{\partial \ln a_{TiO_2}}\right)_{T,\ln a_{O_2}} > 0 \tag{2.29}$$

Now let us suppose that the fixed nonmolecularity is such that

$$K_i^{1/2},\ K_s^{1/5} << -\beta\eta << [A_{Ti}'],\ [D_{Ba}^{\cdot}] \tag{2.30}$$

Then, for the pure undoped case in Fig. 2.3(a), the regime of n=p cannot be seen and the sequence of majority disorder types subsequently turn the same as that in Fig. 2.3(b) whether $K_i^{1/2} >> K_s^{1/5}$ or $K_i^{1/2} << K_s^{1/5}$. The latter is transformed as in Fig. 2.4(a), where it is noted that $[V_{Ti}'''']\approx -\beta\eta$ is flat against log a_{O_2}. For the acceptor-doped case Fig. 2.3(c), the majority disorder regime of $p=4[V_{Ti}'''']$ is impossible because $[V_{Ti}'''']\approx -\beta\eta$ is fixed. Consequently, the transformed plot should be as in Fig. 2.4(b). For the donor-doped case of Fig. 2.3(d), the majority disorder regime $[D_{Ba}^{\cdot}]=4[V_{Ti}'''']$ cannot exist due to the assumption on η, Eq. 2.30 and the regime $p=4[V_{Ti}'''']$ either for the same reason as in the acceptor-doped case. Fig. 2.3(d) is, thus, transformed as in Fig. 2.4(c).

Actually, any shift of disorder regime with the component activities is only made possible by exchanging the chemical components, say O and Ti (or Ba) with the surrounding. Otherwise, the shift itself would be impossible. For example, when our donor-doped $BaTiO_3$ undergoes a shift from $[D_{Ba}^{\cdot}]\approx 4[V_{Ti}'''']$ to $n\approx[D_{Ba}^{\cdot}]$ at a fixed a_{TiO_2} (see Fig. 2.3(d)), the lattice molecule changes nominally from $Ba_{1-y}D_yTi_{1-y/4}O_3$ to $Ba_{1-y}D_yTiO_3$, that is, η changes from $-y/4$ to 0, indicating that Ti is supplied from (or Ba is drained to) the surrounding. This is why we have limitations on the availability of the majority disorder regimes for the partially closed cases (η=constant) in Figs. 2.4(b) and (c). One may take advantage of this fact to tell whether the system is closed with respect to metallic component exchange: If a donor-doped $BaTiO_3$ exhibits an a_{O_2}-region where $n\propto a_{O_2}^{-1/4}$ in agreement

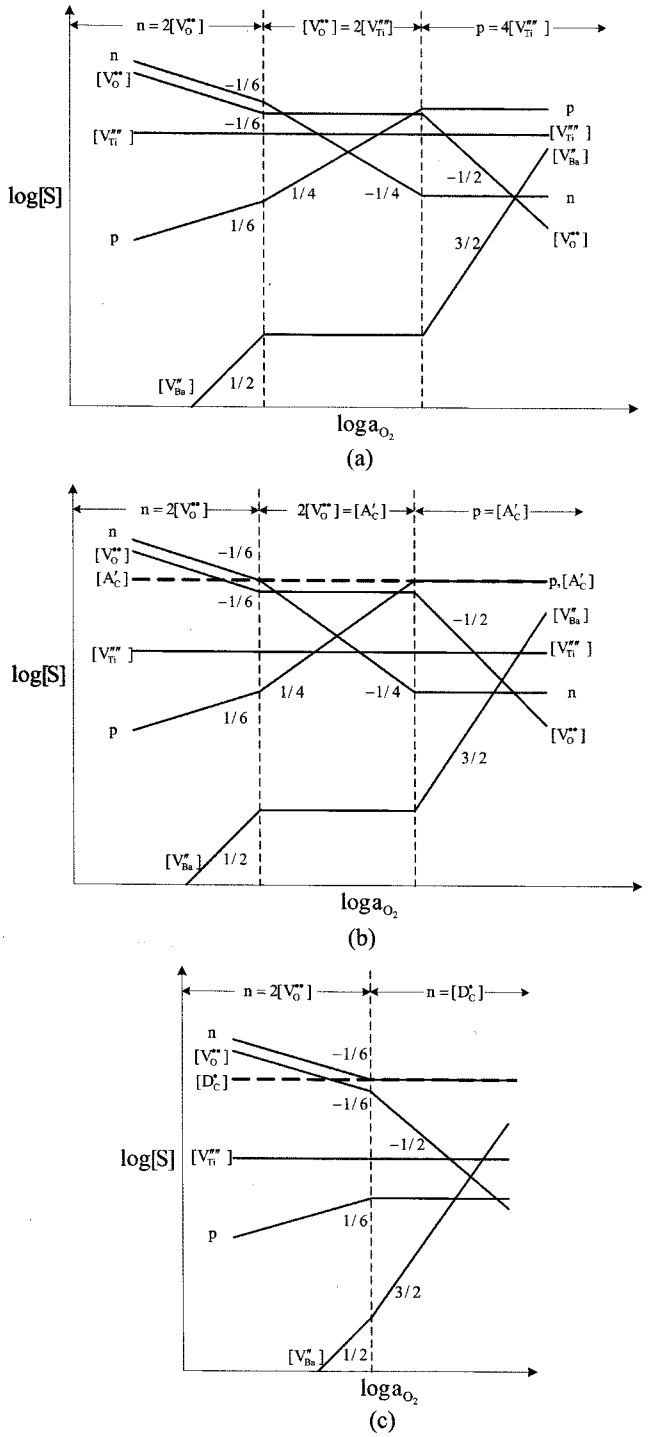

Fig. 2.4. Log [S] vs. log a_{O_2} at fixed nonmolecularity η, (a)-(c) corresponding to Figs. 2.3(b)-(d), respectively.

with Fig. 2.3(d), for example, then one may say that the system remains open to keep a_{TiO_2}, rather than η, constant, indicating the presence of a second phase.[11]

Finally, one may be interested in the variation of a_{TiO_2} with a_{O_2} while η is held fixed. It is calculated via Eq. 2.27 or Eq. 2.6 or more easily in the present case as

$$a_{TiO_2} = K_T'[-\beta\eta]^{-1}[V_O^{\cdot\cdot}]^{-2} \tag{2.31}$$

due to the external equilibrium

$$Ti_{Ti}^x + 2O_O^x = V_{Ti}^{''''} + 2V_O^{\cdot\cdot} + TiO_2 \tag{2.32}$$

that is another aspect of (thus redundant with) Eq. 2.6 or $K_T K_T' = K_S$. One can now draw in Figs. 2.4 (a)-(c) the variations of log a_{TiO_2} simply by following that of $[V_O^{\cdot\cdot}]$, but with twice its slope in the opposite sense.

2.5. A further complication: hole trapping

Up to now, we have considered that all donors or acceptors, whether intrinsic or extrinsic, are fully ionized. As temperature is lowered, however, those centers particularly of extrinsic origin tend to trap electrons or holes. Once electronic carriers are fully trapped, the defect-sensitive properties are often altered appreciably at low temperatures in particular.[7,8] The trapping effect may be ingeniously taken advantage of in designing the composition of actual material for special functions. Here we will consider, for example, hole trapping by fixed-valent acceptor impurities, say, A_{Ti}'.

When hole trapping is no longer negligible and hence, the concentration of the trapped holes, say, $[A_C^x]$ is of concern, one add to Eqs. 2.3-2.6 one more equilibrium condition, that is the internal equilibrium condition with respect to hole trapping or ionization equilibrium condition of the acceptors,

$$A_C^x = A_C' + h^{\cdot} \quad ; \quad K_a = \frac{[A_C']p}{[A_C^x]} \tag{2.33}$$

Mass conservation constraint, Eq. 2.17 is accordingly modified as

$$[A_C'] + [A_C^x] = [A]_t \tag{2.34}$$

The charge neutrality equation, however, remains the same or Eq. 2.18 because the trapped holes make the acceptor centers only neutral (A_C^x) in the present case. Otherwise, it would have to be modified to include the acceptors with different effective charges due to hole trapping.

One may define the trapping factor χ^{-1} as

$$\chi^{-1} \equiv \frac{[A_C^x]}{p} = \frac{[A_C']}{K_a} \tag{2.35}$$

Two extreme cases are distinguished. When $\chi^{-1} << 1$, the concentration hierarchy will be such that

$$[A_C'] \approx [A]_t > p >> [A_C^x] \tag{2.36}$$

and the defect structure is essentially the same as in Fig. 2.3(c) or Fig. 2.4(b) only with $[A_{Ti}^x]$ added as a minority disorder if one likes. When $\chi^{-1} >> 1$, on the other hand, most of holes are trapped and the concentration hierarchy in the near stoichiometry regime ($2[V_O^{\cdot\cdot}] \approx [A_{Ti}']$) turns to

$$[A_C'] \approx [A]_t > [A_C^x] >> p \tag{2.37}$$

As a_{O_2} increases further, the trapped centers come to overwhelm the acceptor impurities or

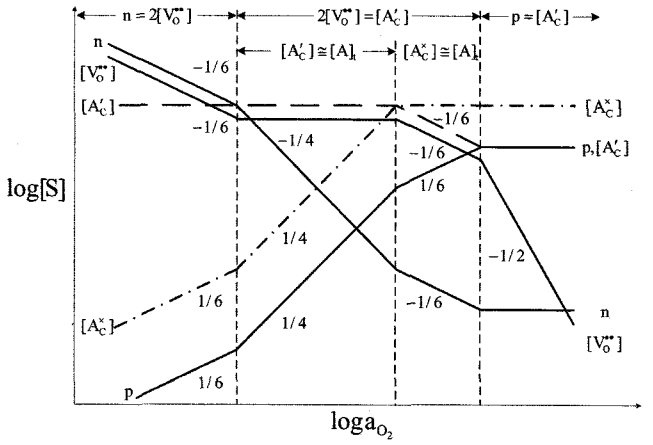

Fig. 2.5. Defect structure for the acceptor-doped case (corresponding to Fig. 2.3(c) or Fig. 2.4(b)) with holes trapped fully ($\chi^{-1}>>1$).

$$[A_C^x]\approx[A]_t >>[A'_C]>p \qquad (2.38)$$

As a_{O_2} increases even further, the charged disorders in majority will finally become $p=[A'_{Ti}]$. The defect structure is as shown in Fig. 2.5, in which the portion corresponding to the concentration hierarchy of Eq. 2.37 is essentially the same as given by Waser[7] for $SrTiO_3$.

2.6. Defect structure and reality

Experimental studies on defect structure of complex oxides are very much limited compared to those on binary systems. It is, thus, fair to say that our understanding of the defect structure of the complex oxides is still far from complete. For example, $BaTiO_3$ is one of the most studied systems, but we still do not know whether donor impurities, say, $La_{Ba}^{\cdot}$ are compensated by $V_{Ti}^{''''}$ or $V_{Ba}^{''}$ or both in the ion-compensation regime. Furthermore, it has been believed from a structural point of view that Ba is more mobile than Ti, but a most recent study[9] shows that Sr substituting Ba and Zr substituting Ti are all comparatively mobile at elevated temperatures, leaving the defect structure more puzzling.

Information on the defect structure has been obtained usually from the observations of defect-structure-sensitive properties against the component activities, say, a_{TiO_2} and a_{O_2}, in particular. The simplest and straightforward properties may be electrical conductivity and (self- or impurity-) tracer diffusivities among others because they are directly proportional to the concentrations of relevant defects in the majority. For the system of $BaTiO_3$, for example, a multitude of studies have been made on the electrical conductivity against a_{O_2}(see, e.g., Ref. 8), but never been done against a_{TiO_2}. The latter may be experimentally extremely difficult to control if not impossible. Cation tracer diffusion study against oxygen activity has just been started.[9] Even for the conductivity studies, it is not always clear whether a_{TiO_2} or η is held fixed during the measurement. The system under examination is, thus, likely ill-defined thermodynamically in the strictest sense.

For the system of $BaTiO_3$, the equilibrium conductivity has been the most extensively documented (see, e.g., Refs. 8, 10 and 11) over the experimentally viable range of $-20<\log a_{O_2}\leq 0$ at elevated temperatures, but the remaining variable, a_{TiO_2} or η has not been explicitly specified. Fig. 2.6 shows the typical results for the pure (a)[10,12], acceptor (A'_{Ti})-doped (b)[13] and donor ($La_{Ba}^{\cdot}$)-doped case (c)[11], respectively.

The conductivity is mostly attributed to electronic carriers, thus proportional to n or p depending on which is in the majority against a_{O_2} and hence, $\sigma_{el}\propto a_{O_2}^{m}$ due to Eq. 2.13 or Eq. 2.28 in each disorder regime. It has always been found for the undoped and acceptor-doped cases all alike that over the entire range of oxygen activity examined, the oxygen exponent "m" takes a value close to $-1/6$, $-1/4$ and $+1/4$ in sequence with increasing a_{O_2}.[8,10] For the acceptor-doped case, this sequential variation is no doubt in agreement with the sequential shift of the majority disorder types from $n\approx 2[V_O^{\cdot\cdot}]$ to $2[V_O^{\cdot\cdot}]\approx[A'_{Ti}]$ with increasing a_{O_2} as shown in Fig. 2.3(c) or Fig. 2.4(b). For the undoped case, however, the interpretation of the same m-sequence is not so straightforward because depending on a_{TiO_2} or η, there can be, next to the $n\approx 2[V_O^{\cdot\cdot}]$ regime where $n\propto a_{O_2}^{-1/6}$, two possible ionic disorder regimes, $[V_O^{\cdot\cdot}]\approx[V_{Ba}^{''}]$ or $[V_O^{\cdot\cdot}]\approx 2[V_{Ti}^{''''}]$ where $n\propto a_{O_2}^{-1/4}$ and $p\propto a_{O_2}^{+1/4}$, see Fig. 2.1(b) and Table 2 or Fig. 2.3(b). It is not clear yet for the system of "pure" $BaTiO_3$, the experimental finding of $\sigma_{el}\propto a_{O_2}^{\pm 1/4}$ is due to $[V_O^{\cdot\cdot}]\approx[V_{Ba}^{''}]$ or $[V_O^{\cdot\cdot}]\approx[V_{Ti}^{''''}]$ or even due to the background impurity acceptors.[8,10] This issue may be elucidated by observing the conductivity variations on pure specimens with different nonmolecularity η, but the experiment may be not so easy because of the extremely limited range of η of the single phase $BaTiO_3$[14,15]. Furthermore, none of the exclusively p-type regimes, ($h^{\cdot}$,A'_C), ($h^{\cdot}$,$V_{Ba}^{''}$) and ($h^{\cdot}$,$V_{Ti}^{''''}$) has ever revealed itself up to $a_{O_2}=1$ for the system of $BaTiO_3$.

For the donor-doped case, on the other hand, the oxygen exponent of the conductivity takes values $m\approx -1/6$, 0, $-1/4$ in sequence as a_{O_2} increases up to 1,[8] see Fig. 2.6(c). This sequence reflects the shift of the majority disorder types from $n\approx 2[V_O^{\cdot\cdot}]$ (m=-1/6) to $n\approx[La_{Ba}^{\cdot}]$ (m=0) and finally to either $[La_{Ba}^{\cdot}]\approx 2[V_{Ba}^{''}]$ or $[La_{Ba}^{\cdot}]\approx 4[V_{Ti}^{''''}]$ (m=−1/4), see Fig. 2.1(d) and Table 2 for the m-values. There seems to be no doubt about the majority disorder types for the former two regimes (m=−1/6 and 0), but the last, ionic compensation regime is not clear concerning whether $[La_{Ba}^{\cdot}]\approx 2[V_{Ba}^{''}]$ or $[La_{Ba}^{\cdot}]\approx 4[V_{Ti}^{''''}]$. There was once an attempt to elucidate this issue: Yoo et al.[11] measured the equilibrium conductivity on the three donor-doped specimens with nominal compositions $Ba_{1-y}La_yTi_{1-y/4}O_3$ (designated as V_{Ti}), $Ba_{1-3y/2}La_yTiO_3$ (as V_{Ba}) and $Ba_{1-y}La_yTiO_3$ (as E) all with y=0.01 for the purpose of sorting out one out of $V_{Ti}^{''''}$, $V_{Ba}^{''}$ and e' that can compensate the impurity donors $La_{Ba}^{\cdot}$ in air atmosphere. The results are as shown in Fig. 2.6(c). It has been found that there is a minority second phase for all the three and the p-type conductivity increases up to 16% of the total electronic conductivity at $a_{O_2}=1$. Consequently, no conclusion could be drawn

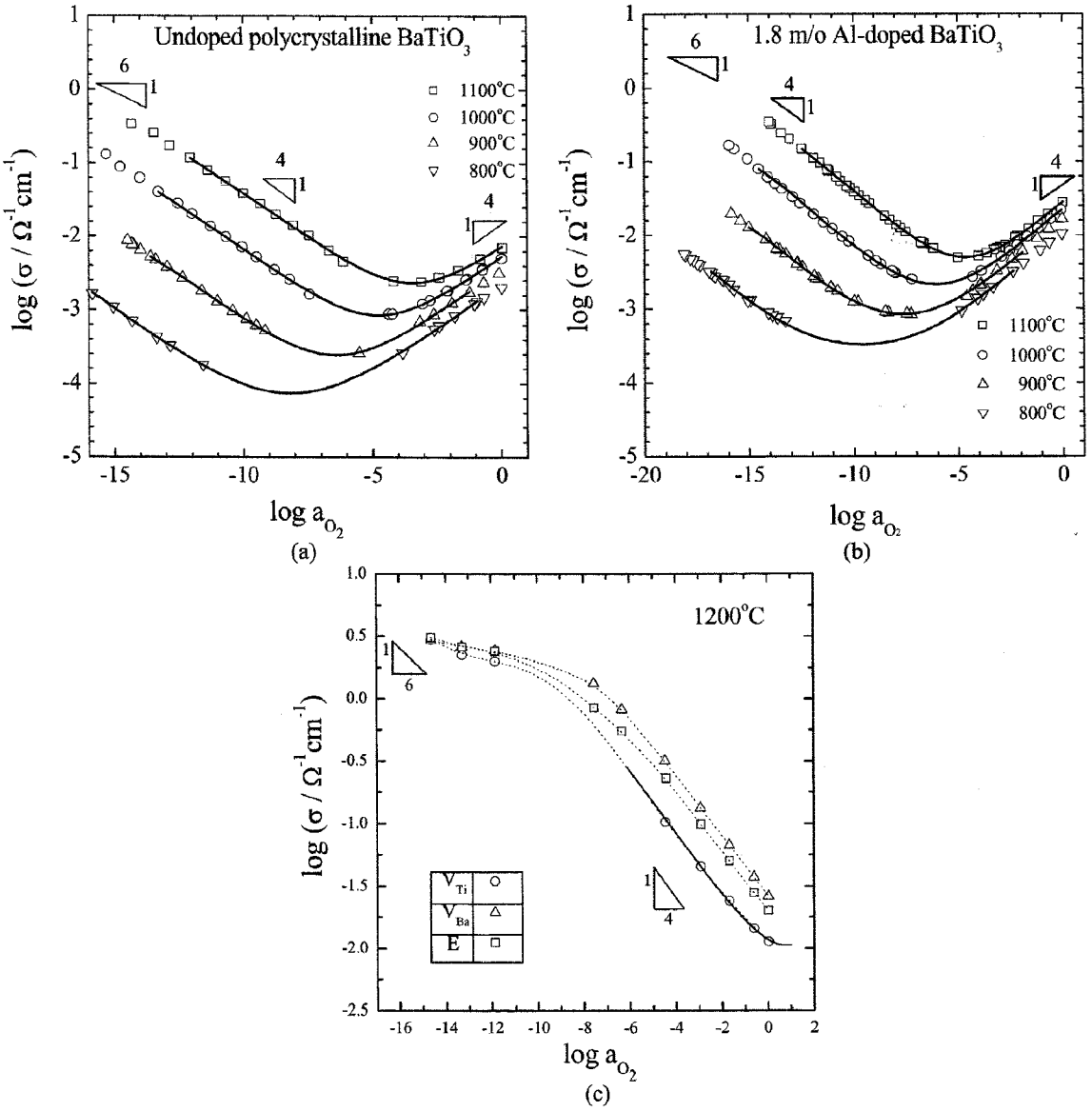

Fig. 2.6. Equilibrium total electrical conductivity(σ) vs. log a_{O_2} of $BaTiO_3$: (a) Undoped, polycrystalline $BaTiO_3$, from Ref. 10; (b) Acceptor(1.8 m/o Al)-doped single crystalline $BaTiO_3$, from Ref. 28; (c) Donor(1.0 m/o La)-doped polycrystalline $BaTiO_3$, from Ref. 11.

to the identity of the ionic disorder compensating the doped donor impurities, but it has been concluded that a_{TiO_2}, rather than η, is held fixed as in Fig. 2.3(d) because the region where $n \propto a_{O_2}^{-1/4}$ and $p \propto a_{O_2}^{+1/4}$ is observed at high oxygen activity region that would otherwise not be seen, see Fig. 2.4(c).

For the quantitative, defect-chemical analyses of all these conductivities in Fig. 2.6, the reader is referred to Refs. 10,11,13,16. It is mentioned in passing that for the case of Al-doped $BaTiO_3$, Fig. 2.6(b), practically all holes are trapped by Al-acceptors at the measurement temperatures.[17] The responsible defect structure is, thus, as given in Fig. 2.5 and the p-type conductivity (m=1/4) in Fig. 2.6(b) is essentially due to the trapped holes[17].

3. Oxygen Nonstoichiometry

Eqs. 2.15, 2.20 and 2.25 indicate that whether the system is undoped or doped, its oxygen nonstoichiometry is a measure of the concentrations of electronic charge carriers, n and p,

$$\beta\delta = \frac{1}{2}(n-p) \tag{3.1}$$

Fig. 3.1 shows how the nonstoichiometry alters the trend of defect-sensitive properties such as the electronic electrical conductivity, thermoelectric power and oxygen chemical diffusivity.[10] Thus, the control of oxygen nonstoichiometry during processing is very often crucial to ensure the required properties of an oxide or functions of the device

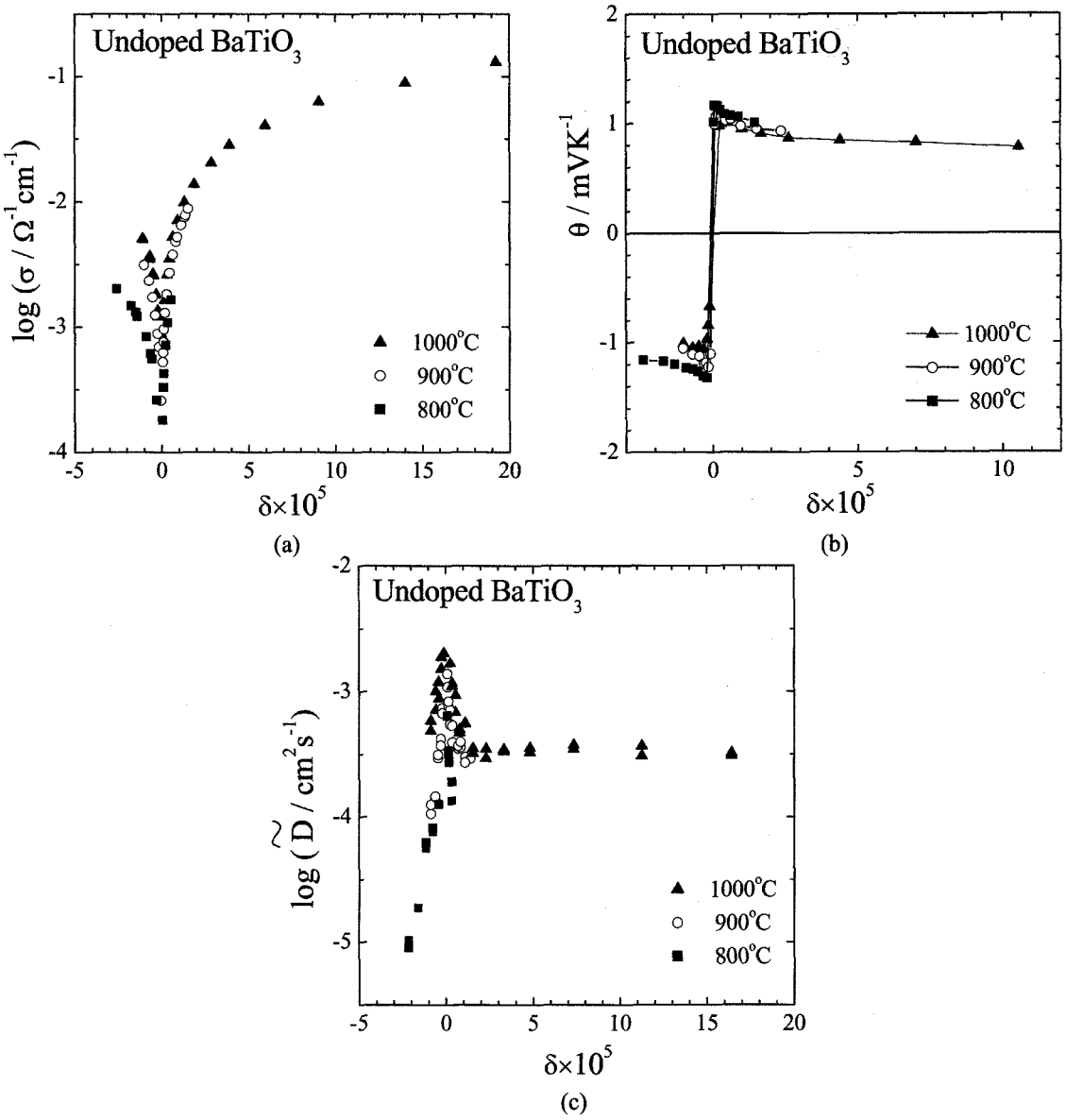

Fig. 3.1. Electrical conductivity (a), thermoelectric power (b) and chemical diffusivity (c) of undoped $BaTiO_{3-\delta}$ vs. oxygen nonstoichiometry δ. Note that the stoichiometric composition is the demarcation point between n-type and p-type behavior. From Ref. 10.

thereof.

As is expected from Fig. 3.1, either in far oxygen-deficit ($\delta>>0$) or oxygen excess region ($\delta<<0$), the nonstoichiometry variation is rather trivial because $n>>p$ or $n<<p$. In the near stoichiometry region $\delta\approx0$, on the other hand, the nonstoichiometry variation is not so trivial because there are both electrons and holes. If electronic carriers are trapped by, e.g., doped impurities, then nonstoichiometry variation is even further informative. We will consider here the most general case, namely, the nonstoichiometry in the near stoichiometry region of the acceptor-doped $BaTiO_3$ with holes trapped.

3.1. Nonstoichiometry in general

For the acceptor-doped $BaTiO_3$ with the lattice molecular formula of Eq. 2.16, the nonstoichiometry has been given as Eq. 2.20 or

$$\beta\delta=[V_{\ddot{O}}]-[V''_{Ba}]-2[V''''_{Ti}]-\frac{1}{2}[A_{Ti}]_t \tag{3.2}$$

When the concentration of trapped holes is no longer negligible compared to that of free holes, one may rewrite Eq. 3.2, due to the mass conservation constraint, Eq. 2.34 and the charge neutrality constraint, Eq. 2.18, as

$$\beta\delta=\frac{1}{2}[n-p-[A^x_{Ti}])=\frac{1}{2}[n-p(1+\chi^{-1})] \tag{3.3}$$

where χ^{-1} is the trapping factor defined as the concentration ratio of trapped holes to free holes in Eq. 2.35. It is noted that the stoichiometric composition $\delta=0$ falls, in general, at

$n=p(1+\chi^{-1})$, not at $n=p$. Only when $\chi^{-1}\rightarrow 0$, the latter would be the case.

The solutions for the defects in Eq. 3.3 are given in the majority disorder regime of $2[V_O^{\cdot\cdot}]=[A'_{Ti}]$ (see Table 2) as

$$p=\chi[A_C^x] \tag{3.4}$$

$$n=K_i\chi^{-1}[A_C^x]^{-1} \tag{3.5}$$

$$[A_C^x]\approx 2^{-1/2}[A]_t^{3/2}K'^{1/2}_{Ox}a_{O_2}^{1/4} \tag{3.6}$$

Eq. 3.3 then takes the form[17],

$$\beta\delta=-\sqrt{K'_i}\sinh\left(\frac{1}{4}\ln\frac{a_{O_2}}{a^{o}_{O_2}}\right) \tag{3.7}$$

where

$$K'_i\equiv K_i(1+\chi^{-1}) \tag{3.8}$$

$$a^{o}_{O_2}=4(1+\chi^{-1})^{-2}K_i^{-2}K_{Re}^2[A]_t^{-2} \tag{3.9}$$

The latter $a^{o}_{O_2}$ is the oxygen activity corresponding to $\delta=0$ or $n=p(1+\chi^{-1})$, see Fig. 2.5. At this specific oxygen activity $a^{o}_{O_2}$, the variation $\beta\delta$ as a function of $\ln a_{O_2}$ exhibits an inflection or

$$\left(\frac{\partial^2(\beta\delta)}{\partial\ln a_{O_2}^{\ 2}}\right)_T=0 \tag{3.10}$$

This fact actually provides a means to locate the stoichiometric point on a nonstoichiometry isotherm that is measured.[18]

Eq. 3.8, in association with Eq. 2.3, indicates that $K'_i=n(p+[A_C^x])$, thus, the latter may be called the "pseudo equilibrium constant for intrinsic electronic excitation." It is noted that only when $\chi^{-1}\rightarrow 0$, $K'_i\rightarrow K_i$ and Eq. 3.7 takes the conventional, familiar form:

$$\beta\delta=-\sqrt{K_i}\sinh\left(\frac{1}{4}\ln\frac{a_{O_2}}{a^{o}_{O_2}}\right) \tag{3.11}$$

This may be the case if the system is pure enough and/or temperature is high enough, see Eq. 2.35. It has often been attempted to determine K_i from the nonstoichiometry isotherms via Eq. (3.11) even for a system which bears possible trapping centers, e.g, acceptor impurities whether they are intentionally doped or not. In any case, one should be aware what he actually determines is not the true K_i, but K'_i in general that is dependent on the type and concentration of the trap centers. One way to evaluate K_i may be to determine K'_i as a function of $[A]_t$ via Eq. 3.7 at fixed temperature or $K'_i=K_i(1+[A]_t/K_a)$, due to Eqs. 3.8, 2.35 and 2.36. Then, one may take its limiting value as $[A]_t\rightarrow 0$ for the true K_i. This, however, has never been experimentally implemented yet.

Once the nonstoichiometry is measured as a function of oxygen activity at different temperatures, the partial molar enthalpy of component oxygen relative to gas oxygen at the standard state, $\Delta\overline{H}_O(=\overline{H}_O-H^{o}_{O_2}/2)$ is of some interest. By noting that the relative partial molar Gibbs free energy of component oxygen $\Delta\overline{G}_O=\mu_O-\mu^{o}_{O_2}/2=RT\ln a_{O_2}^{1/2}$ in Eq. 3.7,

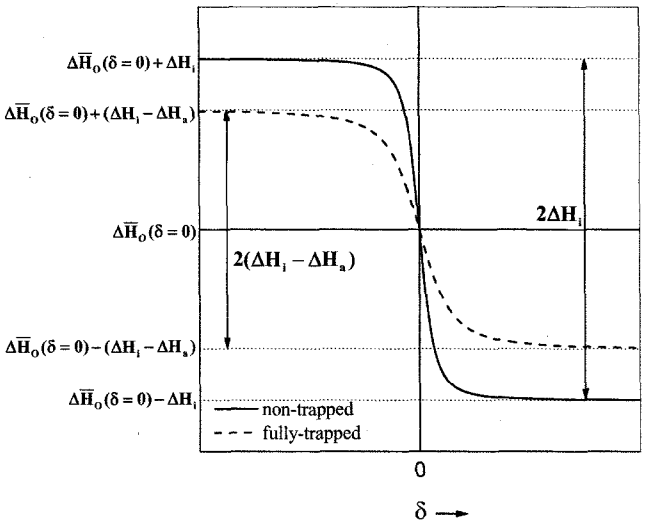

Fig. 3.2. Variation of the relative partial molar enthalpy of component oxygen vs. oxygen nonstoichiometry for non-trapped case ($\chi^{-1}\rightarrow 0$; solid curve) and fully trapped case ($\chi^{-1}\rightarrow\infty$; dashed curve).

one may obtain, due to the Gibbs-Helmholtz equation,

$$\Delta\overline{H}_O(\delta)=\frac{1}{2}\left[\frac{\partial\ln a_{O_2}}{\partial(1/RT)}\right]_\delta=\Delta\overline{H}_O(\delta=0)-\frac{\beta\delta}{\sqrt{(\beta\delta)^2+K'_i}}\Delta H'_i \tag{3.12}$$

with

$$\Delta H'_i\equiv\frac{\partial\ln K'_i}{\partial(1/RT)}=\Delta H_i-\frac{\partial\ln(1+\chi^{-1})}{\partial(1/RT)} \tag{3.13}$$

where $\Delta\overline{H}_O(\delta=0)$ denotes the relative partial molar enthalpy of component oxygen at the stoichiometric composition ($\delta=0$). It is noted that as $\chi^{-1}\rightarrow 0$, Eq. 3.12 converges to that of the pure case corresponding to Eq. 3.11. Variation of $\Delta\overline{H}_O(\delta)$ gainst δ is illustrated in Fig. 3.2 for $\chi^{-1}\rightarrow 0$ (no trapping) and for $\chi^{-1}\rightarrow\infty$ (full trapping), respectively.

It is seen that $\Delta\overline{H}_O(\delta)$ are bounded by $\Delta\overline{H}_O(\delta=0)+\Delta H'_i$ and $\Delta\overline{H}_O(\delta=0)-\Delta H'_i$ as $\delta<<-\sqrt{K'_i}/\beta$ and $\delta>>(\sqrt{K'_i})/\beta$, respectively, and varies anti-symmetrically crossing $\delta=0$.

The sigmoidal variation of $\Delta\overline{H}_O(\delta)$ crossing $\delta=0$ in Fig. 3.2 may be understood from a bit different view point.[19] For simplicity's sake, let us consider the pure $BaTiO_3$ with no traps. Then, oxidation or oxygen incorporation reaction may take place simultaneously in two ways: one is by producing the free holes and the other by consuming free electrons or

$$\frac{1}{2}O_2(g)+V_O^{\cdot\cdot}=O_O^{\times}+2h^{\cdot} \tag{3.14}$$

$$\frac{1}{2}O_2(g)+V_O^{\cdot\cdot}+2e'=O_O^{\times} \tag{3.15}$$

They are indistinguishable thermodynamically, but distinguishable defect-chemically. Letting K_p and K_n denote the equilibrium constant for these reactions, respectively, they are

$$K_p=\frac{p^2}{[V_O^{\cdot\cdot}]a_{O_2}^{1/2}}\quad;\quad K_n=\frac{1}{[V_O^{\cdot\cdot}]n^2a_{O_2}^{1/2}} \tag{3.16}$$

Obviously, $K_n = K_{Re}^{-1} = K_p K_i^{-2}$, see Eqs. 2.3 and 2.5, and hence, the associated enthalpy changes ΔH_p and ΔH_n are interrelated as

$$\Delta H_n = -\Delta H_{Re} = \Delta H_p - 2\Delta H_i \tag{3.17}$$

Given that the oxidation proceeds in this way, $\Delta\overline{H}_O$ may be taken as a fractional sum of ΔH_p and ΔH_n such that

$$\Delta\overline{H}_O = \frac{n}{n+p}\Delta H_n + \frac{p}{n+p}\Delta H_p \tag{3.18}$$

that takes the form, after some algebra using Eqs. 2.3 and 3.1,

$$\Delta\overline{H}_O = \frac{1}{2}(\Delta H_p + \Delta H_n) - \frac{\beta\delta}{\sqrt{(\beta\delta)^2 + K_i}} \cdot \frac{1}{2}(\Delta H_p - \Delta H_n) \tag{3.19}$$

This is essentially the same, due to Eq. 3.17, as Eq. 3.12 with $\chi^{-1} \to 0$. One can then immediately identify $\Delta\overline{H}_O(\delta=0)$ to be

$$\Delta\overline{H}_O(\delta=0) = \frac{1}{2}(\Delta H_p + \Delta H_n) \tag{3.20}$$

If holes are fully trapped or $\chi^{-1} \to \infty$, on the other hand, the oxygen incorporation may proceed via Eq. 3.17 and via, instead of Eq. 3.16,

$$\frac{1}{2}O_2(g) + V_O^{\cdot\cdot} + 2A'_{Ti} = O_O^{\times} + 2A_{Ti}^{\times} \tag{3.21}$$

with the associated enthalpy $\Delta H_p - 2\Delta H_a$, see Eqs. 3.14 and 2.33. In the same line as in Eq. 3.18, one can immediately obtain Eq. 3.12. The same reasoning will also be applied to the case in which electrons are trapped instead of holes.

Eq. 3.18 indicates that when an oxygen atom is incorporated into the lattice, it picks up holes (Eq. 3.14) and electrons (Eq. 3.15) at random depending on their availability. It is, thus, quite natural that the partial molar enthalpy of the component oxygen, $\Delta\overline{H}_O$ is dependent on the relative amount of electrons and holes or the oxygen nonstoichiometry.

The relative partial molar entropy of component oxygen, $\Delta\overline{S}_O$ can also be obtained as a function of δ either by using the thermodynamic identity $[\partial\Delta\overline{G}_O/\partial T]_\delta = -\Delta\overline{S}_O$ or by the same argument as in Eq. 3.18,

$$\Delta\overline{S}_O = \frac{n}{n+p}\Delta S_n + \frac{p}{n+p}\Delta S_p\ , \tag{3.22}$$

but it is not pursued any further. The reader who is interested in is referred to Ref. 19.

3.2. Experimental reality

Nonstoichiometry is normally measured by thermogravimetry or coulometric titrometry. In the former, one changes stepwise the oxygen activity in the surrounding of a specimen oxide and monitor the corresponding weight change. In the latter, one incorporates a predetermined amount of oxygen in the form of ionic current and measure the change in equilibrium oxygen activity in the surrounding. For the experimental details, the reader is referred to, e.g., Refs. 19 and 20. In any case, an extreme care should be exercised in order to secure high enough precision to measure the nonstoichiometry variation particularly in the near-stoichiometry region because the nonstoichiometry variation vs. oxygen activity there is the smallest, see Eq. 3.7 or 3.11. The experimental data are usually scarce in this near stoichiometry region, that is probably for this reason. The stoichiometric point, $a_{O_2}^{\circ}$ in Eqs. 3.7 and 3.11, that is normally determined as in Eq. 3.9, is, thus, not so precisely known for most of oxides whether simple or complex. Here we will show the experimental results on the nonstoichiometry of undoped $BaTiO_3$.

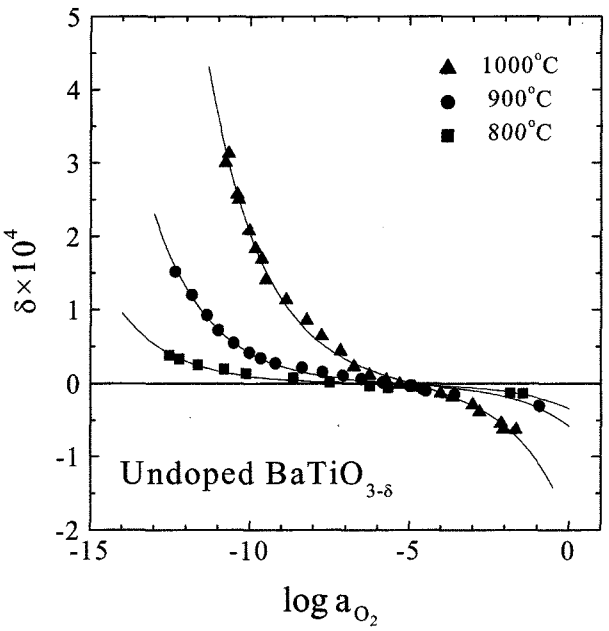

Fig. 3.3. Oxygen nonstoichiometry vs. oxygen activity at different temperatures as measured on undoped $BaTiO_3$. Solid lines are the best fitted to Eq. 3.7 in the text. From Ref. 19.

For the system of undoped $BaTiO_{3-\delta}$, there were five different data sets[21-25] against oxygen activity, that are all limited to the range of log $a_{O_2} < -7$ over the temperature range of 1000°C to 1340°C. Furthermore, only relative changes in nonstoichiometry, not the absolute values, were given.[21,24] Even when the absolute values were reported,[22,23,25] the stoichiometric points could not be located due to the poor precision. It is only recent[19] that the nonstoichiometry has been measured with highest ever precision in the near stoichiometry region including the stoichiometric point $a_{O_2}^{\circ}$. These results are shown in Fig. 3.3.

The solid curves in the figure are the best fitted to Eq. 3.7 with K_i' and $a_{O_2}^{\circ}$ as fitting parameters. As is seen, Eq. 3.7 satisfactorily describes the nonstoichiometry, even though the best-fitted values for the fitting parameters are subjected to rather large uncertainties. The latter is again attributed to the still poor precision of the measurement

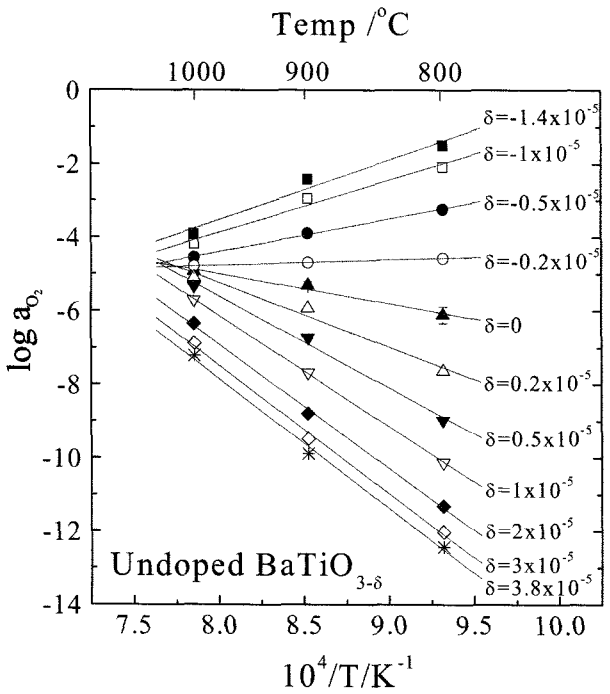

Fig. 3.4. Equilibrium oxygen activity vs. reciprocal temperature at different nonstoichiometry values, see Eq. 3.23 in the text. From Ref. 19.

particularly in the vicinity of the stoichiometric point.

The relative partial molar enthalpy of oxygen is evaluated at different nonstoichiometry values by using the thermodynamic identity

$$\frac{\Delta\bar{G}_O}{RT}=\frac{1}{2}\ln a_{O_2}=\frac{\Delta\bar{H}_O}{RT}-\frac{\Delta\bar{S}_O}{R} \tag{3.23}$$

In Fig. 3.4 is plotted log a_{O_2} vs. reciprocal temperature at different nonstoichiometries. As is seen, it is generally linear for a fixed δ over the temperature range examined. The relative partial molar enthalpy and entropy of oxygen may then be evaluated from the slope and intercept, respectively. The results of $\Delta\bar{H}_O$ are as shown in Fig. 3.5. In agreement with Eq. 3.12, the partial molar enthalpy variation is the best fitted as

$$\Delta\bar{H}_O\,(\delta)/\mathrm{kJmol}^{-1}=-(76\pm5)-\frac{(272\pm38)\delta}{\sqrt{\delta^2+(3.02\pm0.03)\times10^{-11}}} \tag{3.24}$$

4. Nonstoichiometry Re-equilibration

When the oxygen activity is changed in the surrounding of a binary oxide $AO_{1-\delta}$ that has previously been equilibrated with the surrounding, the nonstoichiometry of the oxide changes towards a new equilibrium value. The overall kinetics of this nonstoichiometry re-equilibration process typically consists of the surface reaction step and solid-state-diffusion step in series. The former, gas-sold reaction at the surface is usually regarded as a simple chemical reaction of the first order.[26] The latter diffusion refers to the chemical diffusion of the oxide. We know that there should

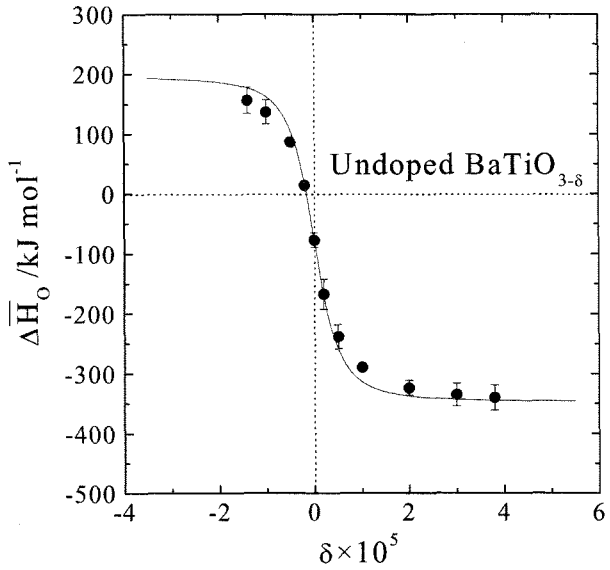

Fig. 3.5. Relative partial molar enthalpy of component oxygen vs. nonstoichiometry for undoped $BaTiO_3$. The solid curve is the best fitted to Eq. 3.12. From Ref. 19.

be one and only chemical diffusion coefficient because there is only one composition variable for the binary oxide (but this is only true when the internal defect equilibrium prevails.[34]).

For an infinite bar of $AO_{1-\delta}$ with the square cross section of $2a\times2a$, for example, the overall re-equilibration kinetics is normally described in terms of the two kinetic parameters, the surface reaction rate constant $\tilde{k}$ and chemical diffusivity $\tilde{D}$ as[12,27]

$$\frac{\bar{\delta}(t)-\delta(0)}{\delta(\infty)-\delta(0)}=1-\left[\sum_{n=1}^{\infty}\frac{2L^2\exp\left(-\frac{\beta_n^2\tilde{D}t}{a^2}\right)}{\beta_n^2(\beta_n^2+L^2+L)}\right]^2 \tag{4.1}$$

with β such that

$$\beta\tan\beta=L\quad;\quad L\equiv\frac{a\tilde{k}}{\tilde{D}} \tag{4.2}$$

Here, $\bar{\delta}(t)$, $\delta(0)$ and $\delta(\infty)$ are the mean (at time t), initial (at t=0) and final (as $t\to\infty$) value of oxygen nonstoichiometry, respectively. By monitoring the temporal variation of the nonstoichiometry $\bar{\delta}(t)$ by thermogravimetry or a δ-sensitive property, e.g., electrical conductivity, thus, one can determine the two kinetic parameters. As far as binary systems are concerned, we believe that we understand the relaxation kinetics well. The chemical diffusion, in particular, has long been understood in the light of chemical diffusion theory[28] or in the light of the ambipolar diffusion theory.[29]

Concerning the complex oxides, however, it is fair to say that the nonstoichiometry relaxation kinetics and chemical diffusion is not so well understood yet. It is only recently that the kinetics has been examined in a systematic way.[12,13,16,30] We will here present the present understanding of the

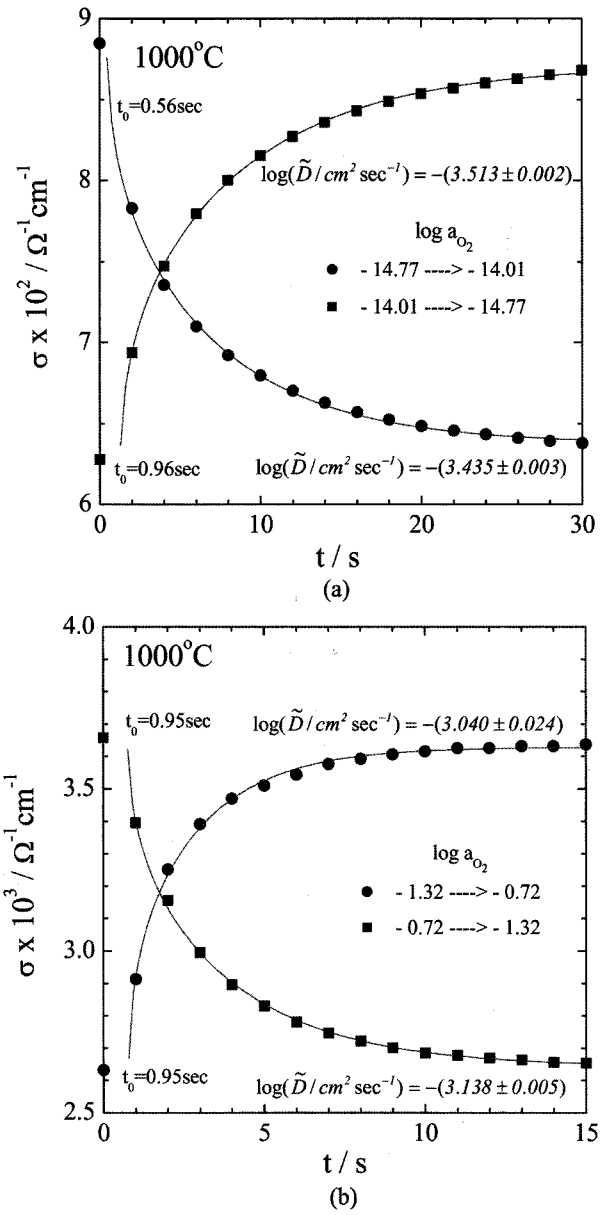

Fig. 4.1. Typical nonstoichiometry relaxation of undoped $BaTiO_3$ in its n-type branch of oxygen activity (a) and p-type branch of oxygen activity (b) during reduction and oxidation at 1000°C. The solid lines are the best-fitted to Eq. 4.1 in the text. From Ref. 12.

kinetics, particularly chemical diffusion process first for the undoped or acceptor doped case and then for the donor doped case, in the order of complexity of the relaxation kinetics.

4.1. Undoped or Acceptor-doped $BaTiO_3$

4.1.1. Relaxation behavior and chemical diffusion

It is already pointed out that the undoped and acceptor doped $BaTiO_3$ have the essentially the same defect structure, Fig. 2.3(c) or 2.4(b), in the oxygen partial pressure range that is experimentally viable in practice, $-18 < \log a_{O_2} \leq 0$. Consequently, the equilibrium conductivities also

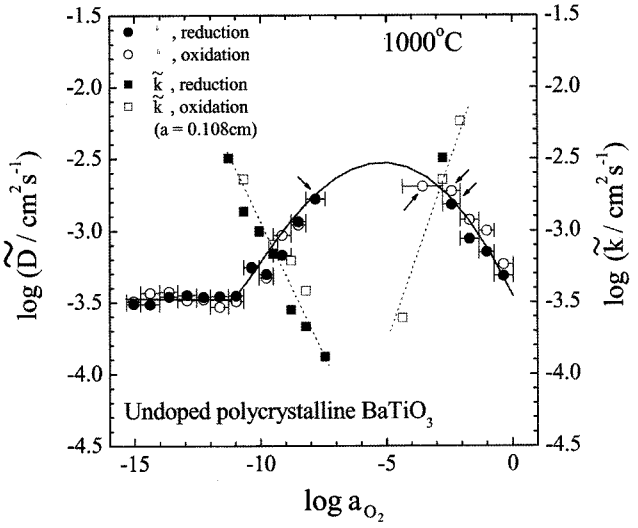

Fig. 4.2. Chemical diffusivity ($\tilde{D}$) and surface-reaction-rate constant ($\tilde{k}$) vs. oxygen activity of undoped $BaTiO_3$ at 1000°C. The dotted and solid lines are for the visual guidance only. From Ref. 12.

have the same trend with oxygen activity as shown in Fig. 2.6(a) and (b). Likewise, the relaxation kinetics has also turned out to be essentially the same.[13,16]

When oxygen partial pressure in the surrounding of the system oxide is abruptly changed either in its n-type branch of oxygen activity ($\sigma_{el} \propto n \propto a_{O_2}^{-1/4}$) or in the p-type branch ($\sigma_{el} \propto p \propto a_{O_2}^{1/4}$) in Fig. 2.6(a) or (b), its electrical conductiviy, as a direct measure of the oxygen nonstoichiometry ($\delta \approx n/2$ or $-p/2$, respectively), relaxes typically as shown in Fig. 4.1 (a) and (b).

These nonstoichiometry relaxations are satisfactorily described by Eq. 4.1, as depicted by the solid curves in Fig. 4.1. The two kinetic parameters are subsequently evaluated as shown in Fig. 4.2.

Upon comparison with the corresponding conductivity in Fig. 2.6(a) or (b), one can see that in the n-p mixed regime of oxygen activity, i.e., in the near vicinity of the conductivity minimum in Fig. 2.6(a) or (b), the overall kinetics is governed mostly by the surface reaction step and otherwise, controlled by the diffusion step. If one totally ignored the surface reaction step or simply took $L \gg 1$ in Eq. 4.1 as was often practiced, he would get, despite somewhat larger uncertainty, a diffusion coefficient which appear as shown in Fig. 4.3.

Finally, the true chemical diffusivities that are responsible for the diffusion step in the nonstoichiometry relaxation kinetics have turned out to be as shown in Figs. 4.4(a) and (b) for the undoped $BaTiO_3$ that is polycrystalline, and for the acceptor (Al)-doped $BaTiO_3$ that is single crystalline, respectively.[12,13] It is noted that the diffusivity takes a value up to the order of 10^{-3} cm^2/s depending on oxygen activity irrespective of temperature in its range examined and exhibits a maximum in the middle of the oxygen activity range examined. One may be concerned that the diffusivity for the polycrystal $BaTiO_3$ (Fig. 4.4(a)) may have been sub-

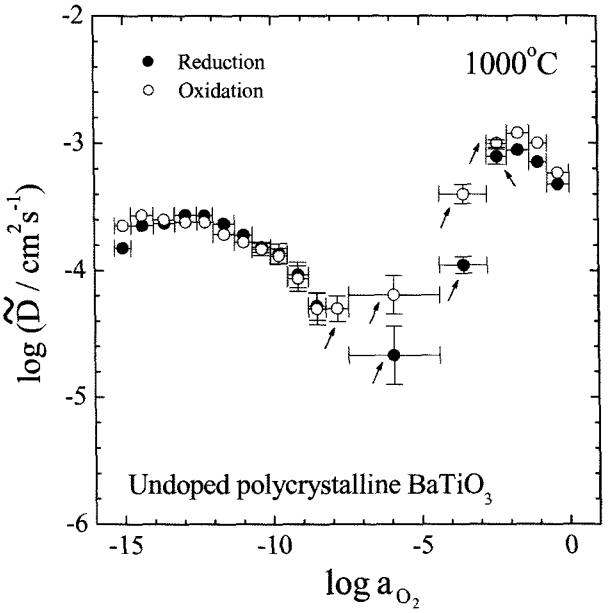

Fig. 4.3. Apparent chemical diffusivity vs. oxygen activity which if the surface reaction step were ignored, would be obtained. From Ref. 12.

jected to the influence of grain boundaries and hence, the diffusivity is somewhat enhanced. It seems not to be the case here, however, because the polycrystal results are quite similar to the single crystal results (Fig. 4.4(b)) in both trend and magnitude.

4.1.2. Defect-chemical interpretation

Referring to the defect structures in Fig. 2.3(c) or 2.4(b) and the corresponding conductivity isotherms in Figs. 2.6(a) and (b), for the undoped and acceptor-doped $BaTiO_{3-\delta}$, respectively, the defects in the majority must be $V_O^{\cdot\cdot}$ compensated by the acceptors A'_C whether they are extrinsic (i.e., A'_{Ti}) or not. One may, thus, take, as the most mobile charged components, oxide ions (O^{2-}) and electrons (e^-) in this near stoichiometry regime.

According to the chemical diffusion theory by C. Wagner,[28] the chemical diffusion coefficient of component oxygen is given as

$$\tilde{D}_O = \frac{RT}{8F^2}\sigma_{ion}t_{el}\left|\frac{\partial[V_O^{\cdot\cdot}]}{\partial \ln a_{O_2}}\right|^{-1} \tag{4.3}$$

where σ_{ion} denotes the partial ionic conductivity, t_{el} the electronic transference number, and F the Faraday constant. The factor within the absolute-value signs is referred to the thermodynamic factor.

Referring to the defect structure in the near stoichiometry regime, $2[V_O^{\cdot\cdot}] \approx [A'_C]$ in Fig. 2.3(c) or 2.4(b), the ionic conductivity is due to $V_O^{\cdot\cdot}$ and essentially independent of oxygen activity. The variation of the total conductivity in Figs. 2.6(a) and (b) is, thus, attributed to that of the partial electronic conductivity, σ_{el} that is due to electrons (e') and holes whether trapped (A^x_{Ti}) or not (h$^{\cdot}$).[17] By using the solutions for n, p and $[A^x_{Ti}]$ in Eq. 2.13 and Table 2, the total conductivities in Figs. 2.6(a) and (b) can be written as[16,17]

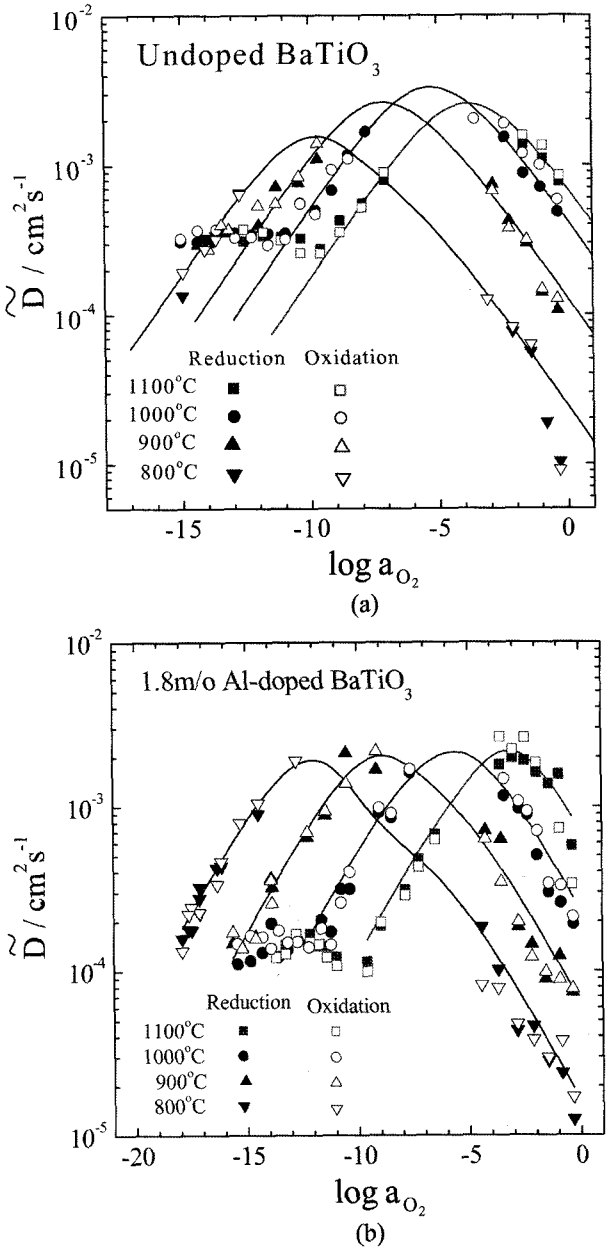

Fig. 4.4. Chemical diffusivity isotherms for the undoped (a) and acceptor (1.8 m/o Al)-doped $BaTiO_3$ (b). From Refs. 13 and 16.

$$\sigma = \sigma_{el} + \sigma_{ion} = \sigma_{el,m}\cosh\left[\frac{1}{4}\ln\frac{a_{O_2}}{a^*_{O_2}}\right] + \sigma_{ion} \tag{4.4}$$

where $\sigma_{el,m}$ denotes the minimum electronic conductivity that falls at the oxygen activity $a^*_{O_2}$, see Figs. 2.6(a) and (b). The solid lines are the best fitted to this equation. By using the values for $\sigma_{el,m}$, $a^*_{O_2}$ and σ_{ion} that are evaluated from σ as the fitting parameters, the electronic transference number t_{el} is calculated as shown in Fig. 4.5 for the case of, e.g., the acceptor-doped $BaTiO_3$.

The thermodynamic factor can also be calculated from the defect strucutre. The oxygen nonstoichiometry is in general given as in Eq. 3.7 or Eq. 3.11. Differentiation leads to the

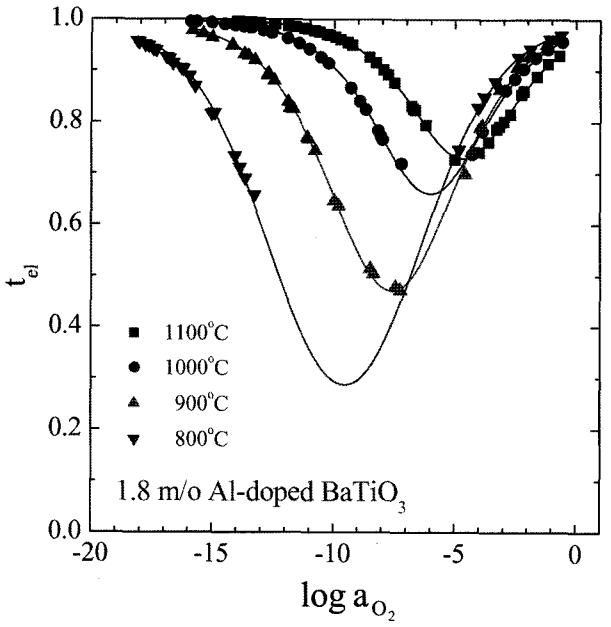

Fig. 4.5. Electronic transference number for 1.8 m/o Al-doped $BaTiO_3$ as calculated from the total conductivity in Fig. 2.6(b). The solid lines are calculated from Eq. 4.4 in the text. From Ref. 13.

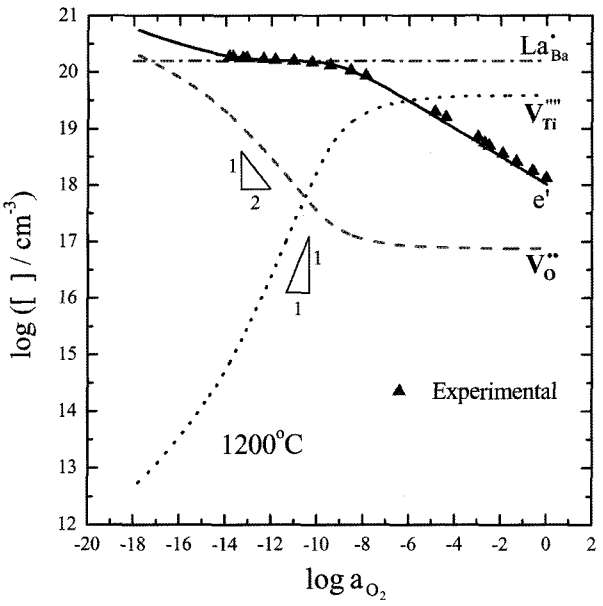

Fig. 4.6. Equilibrium defect structure of 1 m/o La-doped $BaTiO_3$ at 1200°C as derived from the conductivity isotherm. Note that with decreasing oxygen activity, the majority disorder type shift from $[La_{Ba}^{\cdot}] \approx 4[V_{Ti}^{''''}]$ to $[La_{Ba}^{\cdot}] \approx n$ to $n \approx 2[V_O^{\cdot\cdot}]$. From Ref. 30.

thermodynamic factor as

$$\left|\frac{\partial[V_O^{\cdot\cdot}]}{\partial \ln a_{O_2}}\right|^{-1} = \frac{8}{n+p(1+\chi^{-1})} = \frac{4}{\sqrt{K_i'}\cosh\left(\frac{1}{4}\ln\frac{a_{O_2}}{a_{O_2}^o}\right)} \quad (4.5)$$

This is nothing but the inverse of the slope of the nonstoichiometry isotherm as in Fig. 3.3. If the system is pure enough, then one may set $\chi^{-1}=0$. It has been actually found [17] that $\chi^{-1}<<1$ for the undoped, and $\chi^{-1}>>1$ for the Al-doped case.

Finally by substituting Eq. 4.5 into Eq. 4.3, one obtains

$$\tilde{D}_O = \frac{\tilde{D}_O^o t_{el}}{\cosh\left(\frac{1}{4}\ln\frac{a_{O_2}}{a_{O_2}^o}\right)} \quad (4.6)$$

with the factor that is independent of the oxygen activity

$$\tilde{D}_O^o = \frac{RT\sigma_{ion}}{2F^2\sqrt{K_i'}} \quad (4.7)$$

The solid lines in Fig. 4.4 are the best-fitted to Eq. 4.6 by using the experimental values for σ_{ion} and t_{el}.[13,16] As is seen, Eq. (4.6) precisely explains the variation of the chemical diffusivity.

4.2. Donor-doped $BaTiO_3$

4.2.1. Relaxation behavior and chemical diffusion

The nonstoichiometry relaxation of the undoped or acceptor-doped $BaTiO_3$ is simple, governed by the chemical diffusion of oxygen and the gas/solid oxygen exchange reaction. It is not different from ordinary binary oxides. This is no longer the case for the donor-doped case. Actually, a long-standing, notorious problem with $BaTiO_3$ (as well as with any other perovskite oxide) is that kinetics of oxygen nonstoichiometry re-equilibration is usually very much, and sometimes even prohibitively, sluggish for donor-doped $BaTiO_3$, compared to undoped or acceptor doped counterparts, and hence, one often hardly knows even whether a donor-doped specimen has been completely equilibrated upon re-equilibration. According to a report,[31] for instance, it took more than 4 months to equilibrate a donor(Nb)-doped $BaTiO_3$ specimen measuring 4 mm×4 mm×12 mm with an average grain size of a few microns upon a change of temperature from 1308 to 1216 K in an atmosphere of fixed oxygen partial pressure of 0.0022 atm. If undoped or acceptor-doped, it would have taken no more than a few hundreds seconds, see Fig. 4.1. This unusually sluggish kinetics may be called the kinetic anomaly of donor-doped $BaTiO_3$. Not surprisingly, the chemical diffusivity data are extremely sparse for donor-doped case. Only two data sets are found in the literature, one by Wernicke[32] on La-doped and the other by Nowotny and Rekas[31] on Nb-doped $BaTiO_3$, both only against temperature in fixed Po_2 atmospheres (0.32 and 0.0022 atm, respectively).

A recent study[30] shows that compared to that of the undoped counterpart in Figs. 4.1 that is usual, the relaxation behavior of donor-doped $BaTiO_3$ appears unusual depending on the oxygen activity.

It is brought back to the reader's attention that in Fig. 2.6(c), the conductivity for the specimen denoted as V_{Ti} is the equilibrium conductivity of La-doped $BaTiO_3$ (nominal composition $Ba_{0.99}La_{0.01}Ti_{0.9975}O_3$), that has an average grain size of 0.86±0.03 μm and the bulk density of 96% of the the-

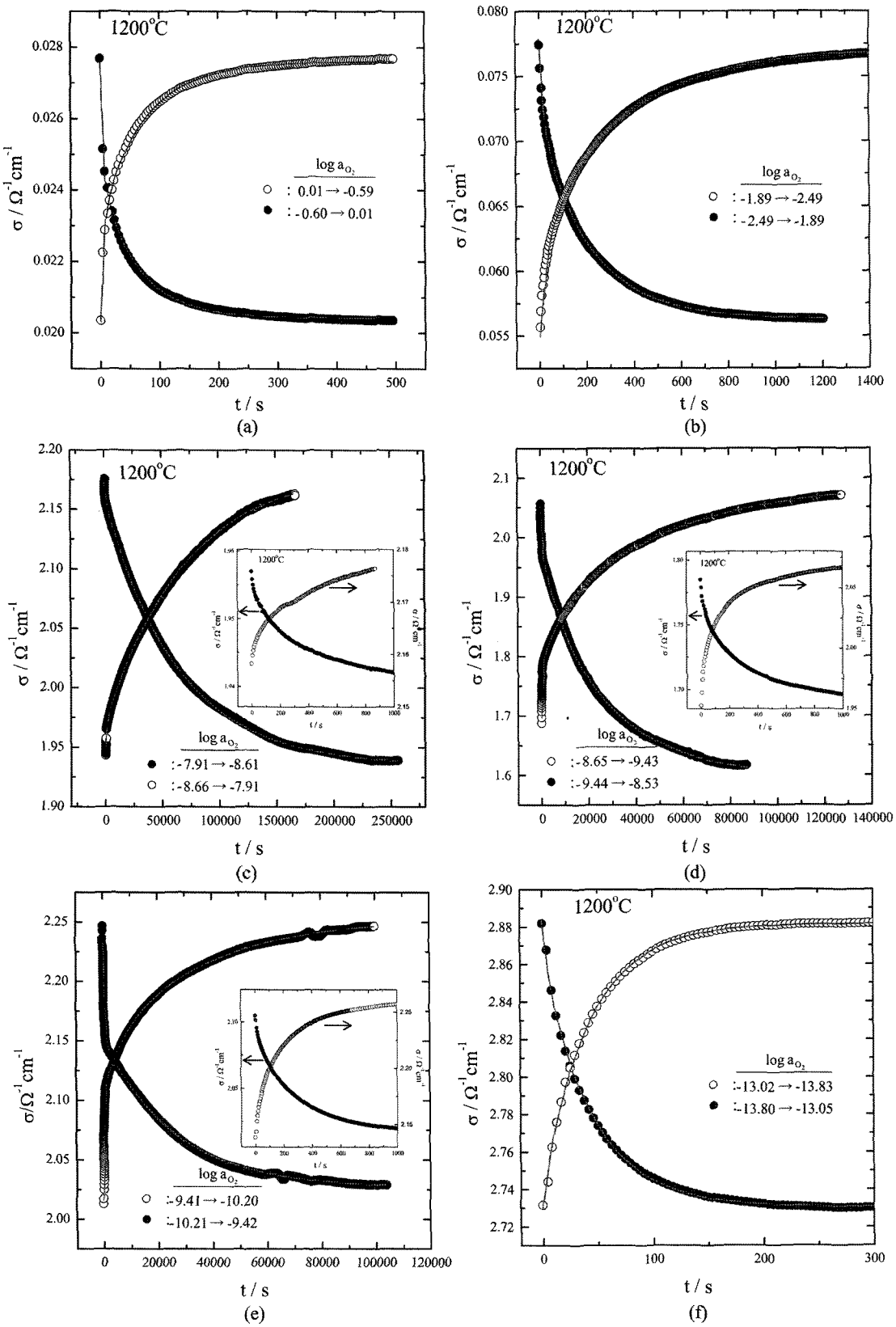

Fig. 4.7. Conductivity relaxation for the stepwise changes back and forth between the oxygen activities (in log a_{O_2}): (a) 0.01↔−0.59; (b)–1.89↔−2.49; (c) −7.91→−8.61 and −8.66→−7.91; (d)–8.65→−9.43 and −9.44→−8.53; (e) −9.41→−10.20 and −10.21→−9.42; (f) −13.02→−13.83 and −13.80→−13.05. Insets: exploded view of the first and faster relaxation. Note the change of kinetics from one-fold (a,b) to two-fold (c-e) to one-fold (f) as the mean oxygen activity decreases. Solid curves are the best fitted to Eq. 4.1 or Eq. 4.11 or Eq. 4.12 in the text. From Ref. 30.

oretical value. The corresponding defect structure is basically as shown in Fig. 2.3(d) and in more detail for the system in present concern, in Fig. 4.6: As Po_2 decreases from 1 atm at the given temperature, the majority type of disorder shifts from $[La_{Ba}^{\cdot}]\approx 4[V_{Ti}^{''''}]$, through $[La_{Ba}^{\cdot}]\approx n$, to $n\approx 2[V_O^{\cdot\cdot}]$.

Fig. 4.7(a)-(f) show sequentially the as-measured conductivity relaxation curves for stepwise changes back (reduction) and forth (oxidation) between the pre-fixed oxygen activities specified, as the (geometric) mean oxygen activity decreases. Clearly, the relaxation behaviors differ depending on the oxygen activity windows imposed or the mean oxygen activity. As the latter decreases from $\log a_{O_2}=0$, the conductivity relaxes apparently with one relaxation time (a,b), with two relaxation times (c-e) and again with one relaxation time (f). In other words, the kinetics varies from 1-fold to 2-fold to 1-fold with decreasing a_{O_2}. The 1-fold and 2-fold kinetics can be more clearly recognized from a plot of the relaxation curves $\sigma(t)$ against log t, instead of t, see Fig. 4.8. It is noted in two-fold kinetics cases [Fig. 4.7(c)-(e)] that the two relaxation times differ by orders of magnitude.

4.2.2. Defect chemical interpretation

The two-fold relaxation is understood as follows: The nonmolecularity η as well as oxygen nonstoichiometry δ of the system is presumed to be spatially homogeneous in the beginning. As soon as a different oxygen activity is imposed upon such a homogeneous system, a new redox equilibrium will be immediately established at the surface of the specimen via the redox reaction, Eq. 2.5, assuming the surface reaction is fast enough (Of course, this is not always the case though[26]), and proceeds inward via chemical diffusion of component oxygen as is the case with the undoped or acceptor-doped $BaTiO_3$.

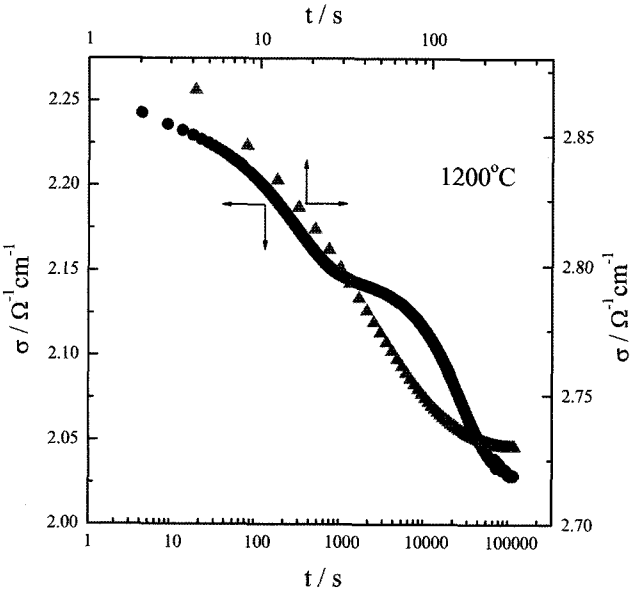

Fig. 4.8. Conductivity vs. time in a log scale. Note the one-fold and two-fold kinetics are clearly discerned, and if $\tau_{Ti}>>\tau_O$, the two-fold kinetics may turn like the one-fold one. From Ref. 30.

Now, we further assume that there also prevails initially the external equilibrium with respect to Ti-exchange (or Ba) between the system and a minority second phase or Eq. 2.6. The presence of the second phase has earlier been indicated upon shifting of the majority disorder types in the donor-doped case[11], see Section 2. Such a second phase, however small it is, holds a_{TiO_2} fixed. When the oxygen activity is suddenly changed to, say, a smaller value, while a_{TiO_2} is fixed by the presence of the second phase, then due to the equilibrium condition Eqs. 2.4 and 2.6 (or $[V_{Ti}^{''''}][V_O^{\cdot\cdot}]^2=K_T a_{TiO_2}$), a gradient of $[V_{Ti}^{''''}]$ is established right at the surface where the surface reaction is again assumed to be fast enough. This gradient subsequently drives the chemical diffusion of, say, component Ti. The thermodynamic situation is depicted in Fig. 4.9.[30]

It is well known that charge neutrality may break down at grain boundaries and surfaces. What is observed in the relaxation of Fig. 4.7, however, is a spatial average property of the specimen, not a local property and hence, the space charge effect may be neglected (i.e., the Debye length is assumed to be sufficiently small compared to the grain size.) The overall charge neutrality condition may then be written for the present case (see Eq. 2.23) as

$$n=[La_{Ba}^{\cdot}]+2[V_O^{\cdot\cdot}]-4[V_{Ti}^{''''}] \tag{4.8}$$

Neglecting the mobility of the donor impurities $La_{Ba}^{\cdot}$, temporal variation of the electronic carrier density n may be written as

$$\frac{\partial n}{\partial t}=2\frac{\partial[V_O^{\cdot\cdot}]}{\partial t}-4\frac{\partial[V_{Ti}^{''''}]}{\partial t}=-2\nabla J_{V_O^{\cdot\cdot}}+4\nabla J_{V_{Ti}^{''''}} \tag{4.9}$$

As the present system is essentially an electronic conduc-

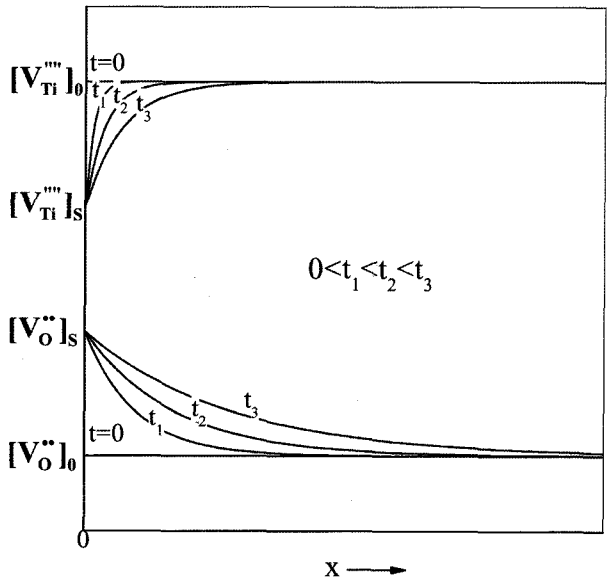

Fig. 4.9. Thermodynamic situation and expected diffusion profiles of $[V_O^{\cdot\cdot}]$ and $[V_{Ti}^{''''}]$ with time upon an abrupt change of oxygen activity at the surface of a specimen x=0. Note that the surface is assumed to be always in equilibrium so that $[V_{Ti}^{''''}][V_O^{\cdot\cdot}]^2$=const. and $D_{Ti}<<D_O$. From Ref. 30.

tor (electronic transference number, $t_{el}\approx 1$) over the entire a_{O_2} range of the present concern, as is clearly seen from Fig. 4.6, the local electroneutrality field will be negligible. Hence, diffusion of each type of ionic defects proceeds in the respective sublattices with no mutual coupling or

$$J_{V_O^{\cdot\cdot}} = -\tilde{D}_O \nabla[V_O^{\cdot\cdot}] \quad ; \quad J_{V_{Ti}^{''''}} = -\tilde{D}_{Ti} \nabla[V_{Ti}^{''''}] \tag{4.10}$$

where $\tilde{D}_O$ and $\tilde{D}_{Ti}$ are the chemical diffusivity of component O and Ti, respectively.

Assuming these chemical diffusivities to be constant for small jumps of oxygen activity, one may obtain the solution to Eq. 4.9 associated with Eq. 4.10 for the initial and boundary conditions given in Fig. 4.9 as

$$\frac{\bar{\sigma}-\sigma_\infty}{\sigma_o-\sigma_\infty} = \frac{\bar{n}-n_\infty}{n_o-n_\infty} = \sum_{k=O,Ti} A_k \frac{8}{\pi^2} \sum_{j=0}^{\infty} \frac{1}{(2j+1)^2} \exp\left[-\frac{(2j+1)^2\pi^2 \tilde{D}_k t}{4a^2}\right] \tag{4.11}$$

with

$$A_O \equiv \frac{2([V_O^{\cdot\cdot}]_o - [V_O^{\cdot\cdot}]_\infty)}{2([V_O^{\cdot\cdot}]_o - [V_O^{\cdot\cdot}]_\infty) - 4([V_{Ti}^{''''}]_o - [V_{Ti}^{''''}]_\infty)} ; \tag{4.12}$$

$$A_{Ti} \equiv \frac{-4([V_{Ti}^{''''}]_o - [V_{Ti}^{''''}]_\infty)}{2([V_O^{\cdot\cdot}]_o - [V_O^{\cdot\cdot}]_\infty) - 4([V_{Ti}^{''''}]_o - [V_{Ti}^{''''}]_\infty)} \tag{4.13}$$

where $\bar{\sigma}$, σ_o and σ_∞ are the mean conductivity at time t, the initial equilibrium conductivity at t=0 and the final equilibrium one as $t\rightarrow\infty$, respectively, $\bar{n}$, n_o and n_∞ the corresponding densities of carrier electrons, and "2a" the thickness of the present specimen that may be regarded as an infinite slab in the present case.

It is noted that $A_O + A_{Ti} = 1$ and their ratio $R(=A_{Ti}/A_O)$ may be regarded as a measure of the relative contribution of Ti-diffusion and O-diffusion processes to the overall re-equilibration kinetics given the relaxation times ($\tau_k = 4a^2/\pi^2\tilde{D}_k$): If R>>1 or R<<1, the conductivity relaxation kinetics may be represented essentially by either τ_{Ti} or τ_O, respectively, that is, one-fold kinetics follows. Otherwise, the kinetics may have to be represented by both τ_{Ti} and τ_O, that is, two-fold kinetics.

The equilibrium defect structure for the present case is calculated to be as shown in Fig. 4.6.[30] In oxidizing atmospheres (say, log $a_{O_2}>-8$) where the majority type of disorder is $4[V_{Ti}^{''''}] \approx [La_{Ba}^{\cdot}] >> [V_O^{\cdot\cdot}]$, $R = |\Delta[V_{Ti}^{''''}]/\Delta[V_O^{\cdot\cdot}]| = 2[V_{Ti}^{''''}]/[V_O^{\cdot\cdot}] \approx 2[La_{Ba}^{\cdot}]/[V_O^{\cdot\cdot}] >> 1$ due to Eqs. 2.4 and 2.6 (or $[V_{Ti}^{''''}][V_O^{\cdot\cdot}]^2 = K_T a_{TiO_2}$); in reducing atmospheres (say, log $a_{O_2}<-13$) where $n\approx 2[V_O^{\cdot\cdot}] >> [V_{Ti}^{''''}]$, $R = 2[V_{Ti}^{''''}]/[V_O^{\cdot\cdot}] << 1$. In these Po_2 regimes, the conductivity relaxation kinetics should appear to be 1-fold or with a single relaxation time, namely, τ_{Ti} and τ_O, respectively. In the intermediate oxygen activity region, then, the overall kinetics may appear two-fold. Thus, the kinetics will have to shift from 1-fold (τ_{Ti}) to 2-fold (τ_{Ti}, τ_O) to 1-fold (τ_O) as oxygen activity decreases from $a_{O_2}=1$.

This is believed to be what has been observed in Fig. 4.7. If it is the case, then one may fit the relaxation data to Eq. 4.11 to evaluate the chemical diffusivities. In the one-fold kinetics region of τ_{Ti}, all the relaxation data could be sufficiently precisely fitted to Eq. 4.11 with $A_O\approx 0$, as depicted by the solid curves in Figs. 4.7(a) and (b), thus, indicating that the rate of surface reactions, Eqs. 4.1 and 4.2 are indeed fast enough compared with the chemical diffusion.

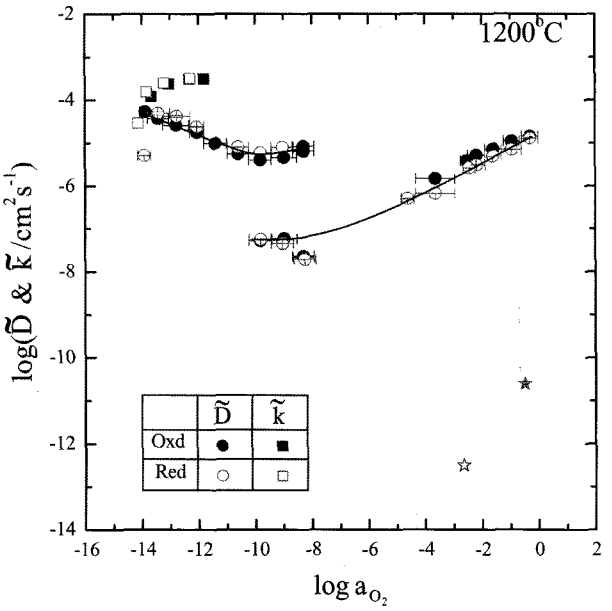

Fig. 4.10. $\tilde{D}_{Ti}$, $\tilde{D}_O$ and $\tilde{k}$ (for oxygen exchange) vs. oxygen activity at 1200°C as evaluated by using the specimen dimension as the decisive diffusion length. ★, D_{Ba} from Ref. 32; ☆, D_{Ti} from Ref. 31.

However, in the one-fold kinetics region of τ_O in the reducing atmospheres, the surface reaction step has to be taken into appropriate account, as in the undoped or acceptor-doped cases,[12,13,26] for a sufficient precision of the fitting. The relaxations are, thus, fitted (solid lines in Fig. 4.7(a-e)) to the conventional solution similar to Eq. 4.1, but in 1-dimension to evaluate $\tilde{D}_O$ and the surface reaction rate constant $\tilde{k}$ simultaneously.

All the results, $\tilde{D}_{Ti}$, $\tilde{D}_O$ and $\tilde{k}a$ (for oxygen exchange) as obtained in this way are compiled in Fig. 4.10. As is seen, $\tilde{D}_O$-values are on the order of magnitude of $-6\sim-4$ (in cm^2/s) depending on oxygen activity. Upon comparison with the $\tilde{D}_O$-values for the undoped and acceptor-doped in Fig. 4.4, one can recognize that the present $\tilde{D}_O$ values are quite reasonable as the chemical diffusivity of oxygen in $BaTiO_3$. In addition, the surface reaction rate constants "$\tilde{k}$" are also comparable in magnitude as well as in trend with those for the undoped or acceptor-doped systems,[26] see Fig. 4.2.

Here, however, one should note that the values for $\tilde{D}_{Ti}$, being in the range of $10^{-8}\sim10^{-5}$ cm^2/s, seem too large in comparison with the two reported values for the chemical diffusivity of the cations in $BaTiO_3$.[31,32] see Fig. 4.10. Remembering that in the evaluation of $\tilde{D}_{Ti}$ via Eq. 4.11, the specimen thickness 2a (=1.2 mm) has been employed as the decisive diffusion length, it indicates that the decisive diffusion length should rather be the grain size than the specimen

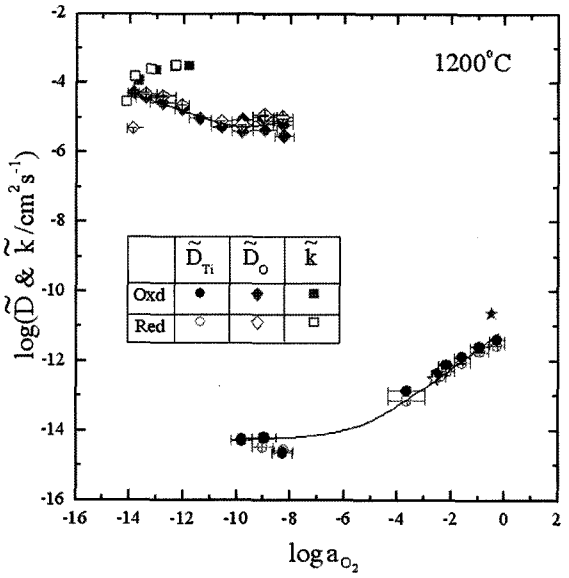

Fig. 4.11. Chemical diffusivities re-evaluated by taking as the decisive diffusion length the sample dimension for D_O and the mean grain size for D_{Ti}. ★, D_{Ba} from Ref. 32; ☆, D_{Ti} from Ref. 31.

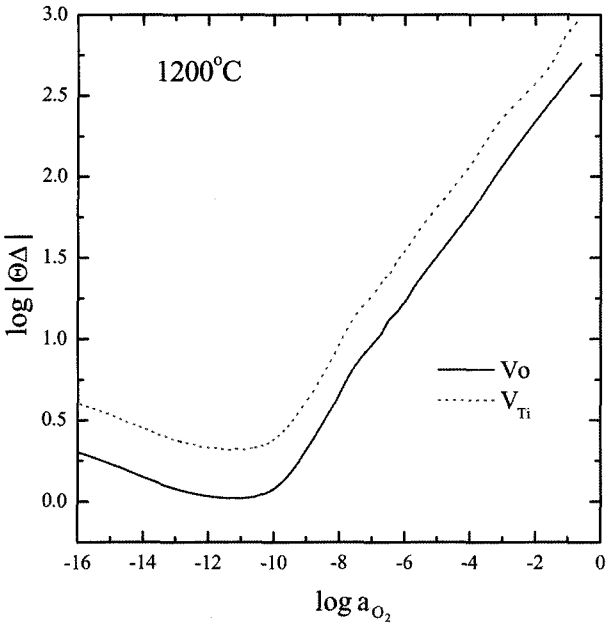

Fig. 4.12. Thermodynamic factors (|ΘΔ|) for O (solid line) and Ti (dotted line) vs. oxygen activity as evaluated from the equilibrium defect structure of 1 m/o La-doped $BaTiO_3$ in Fig. 4.6. From Ref. 30.

thickness.

Simply assuming that the specimen consists of spherical grains with a mean radius "α," Eq. 4.11 is modified to be[27]

$$\frac{\bar{\sigma}-\sigma_\infty}{\sigma_o-\sigma_\infty}=A_O\frac{8}{\pi^2}\sum_{j=0}^{\infty}\frac{1}{(2j+1)^2}\exp\left[-\frac{(2j+1)^2\pi^2\tilde{D}_O t}{4a^2}\right]$$
$$+A_{Ti}\frac{6}{\pi^2}\sum_{j=1}^{\infty}\frac{1}{j^2}\exp\left[-\frac{j^2\pi^2\tilde{D}_{Ti}t}{\alpha^2}\right] \quad (4.12)$$

Reanalyzing all the experimental data for the two-fold kinetics region and higher oxygen partial pressure region to this modified solution (solid lines in Fig. 4.7(a-e)), one obtains the results as shown in Fig. 4.11 along with all those literature data.[31-33]

As is seen, the re-evaluated values are now in a satisfactory agreement with the reported chemical diffusivity values.[31,32] It may, thus, be concluded that the two-fold kinetics is due to the chemical diffusion of oxygen and cation, say, Ti, the chemical diffusivities of which differ by ca. 8 orders of magnitude from each other.

In sum, what happens in the donor-doped $BaTiO_3$ is that the oxygen sublattice has first been equilibrated with a decisive diffusion length of the overall specimen dimension, and the cation sublattice subsequently starts to re-equilibrate from grain surfaces, that is, with the grain size as the decisive diffusion length. Whether or not the two-fold kinetics is observed, seems to be determined by the combination of the relaxation times: If they are not much different, say, let $\tau_O \approx \tau_{Ti}$ or in other words, $2a/\alpha \approx \sqrt{\tilde{D}_O/\tilde{D}_{Ti}}$, then it would not be possible to observe or discern the two-fold kinetics irrespective of the amplitude ratio $R(=A_{Ti}/A_O)$ in Eq. 4.12. For the specimen in question, $2a/\alpha \approx 10^3$ and $\sqrt{\tilde{D}_O/\tilde{D}_{Ti}} \approx 10^4$, thus, observable.[30] If $\tau_O \ll \tau_{Ti}$, the two-fold kinetics should be observed in principle, but no matter what R value is, it would take too long to observe, or there would be little symptom of the cation sublattice relaxation in experimentally viable time. If $R \ll 1$, on the other hand, the cation sublattice relaxation can hardly be detected experimentally, even if there occurs the relaxation. This may be the case of undoped or acceptor-doped $BaTiO_3$ where the kinetics only

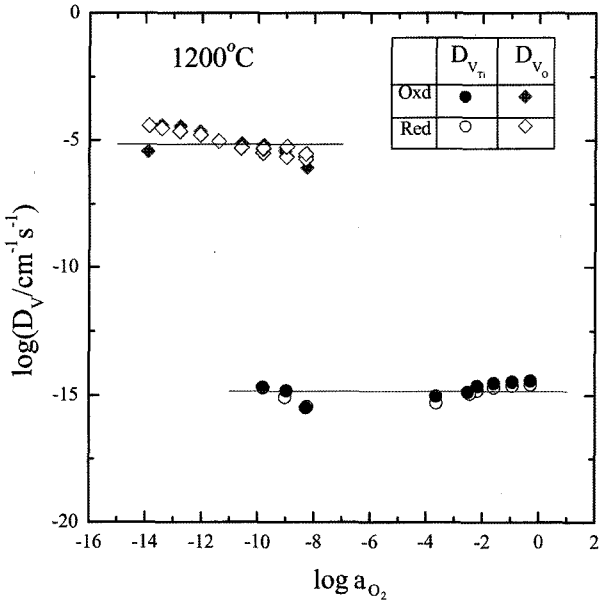

Fig. 4.13. Defect diffusivities of O and Ti vacancies, D_{V_O} and $D_{V_{Ti}}$ vs. oxygen activity at 1200°C. The solid lines, the average values.

appears one-fold and very fast.

4.3. Defect Diffusivities

Again according to Wagner,[28] the chemical diffusivities in Eq. 4.10 may be written for an electronic conductor system ($t_{el} \approx 1$) as

$$\tilde{D}_O = -D_{V_O}\left(\frac{\partial \mu_O}{RT\partial \ln[V_{\ddot{O}}]}\right) = -\frac{D_{V_O}}{2}\left(\frac{\partial \ln a_{O_2}}{\partial \ln[V_{\ddot{O}}]}\right) \quad (4.13)$$

and

$$\tilde{D}_{Ti} = -D_{V_{Ti}}\left(\frac{\partial \mu_{Ti}}{RT\partial \ln[V_{Ti}^{''''}]}\right) = D_{V_{Ti}}\left(\frac{\partial \ln a_{O_2}}{\partial \ln[V_{Ti}^{''''}]}\right) \quad (4.14)$$

due to the identity $\nabla\mu_{Ti} + 2\nabla\mu_O = \nabla\mu_{TiO_2} = 0$ in the presence of the second phase. The quantities within the parentheses, the thermodynamic factors are nothing but the inverses of slopes of the curves for $[V_{\ddot{O}}]$ and $[V_{Ti}^{''''}]$, respectively, in Fig. 4.6. They are graphically evaluated as in Fig. 4.12.

On the basis of Eqs. 4.13 and 4.14, one can, then, evaluate the defect-diffusivities of $V_{\ddot{O}}$ and $V_{Ti}^{''''}$, D_{V_O} and $D_{V_{Ti}}$, respectively. The results are finally as shown in Fig. 4.13. As is seen, each defect diffusivity turns out to be fairly flat against oxygen activity, as expected. Their values at 1200°C, $D_{V_O} = 1.4 \times 10^{-5}$ cm^2/s ; $D_{V_{Ti}} = 1.4 \times 10^{-15}$ cm^2/s are quite reasonable in magnitude, upon comparison with the literature values if available. It should be pointed out that defect diffusivity of the cation vacancy has been evaluated for the very first time in $BaTiO_3$ and the like. Nevertheless, it is still yet to be elucidated which of $V_{Ti}^{''''}$ or $V_{Ba}^{''}$ is in the majority, and which is more mobile whether doped or undoped. It has usually been believed that Ti^{4+} is immobile relative to Ba^{2+} for the energetic reason.[33] A recent study,[9] however, shows that the impurity diffusivities of Sr, that is replacing Ba, and Zr, that is replacing Ti, are comparable to each other.

Acknowledgments

The author thanks C.E. Lee for all the art works. This work was supported partially by the Center for Advanced Materials Processing under the "21C Frontier Program" and by "Core Technology Development Program for Fuel Cells" both of the Ministry of Commerce, Industry & Energy, Korea.

REFERENCES

1. R. Wernicke, "The Influence of Kinetic Processes on the Electrical Conductivity of Donor-doped $BaTiO_3$ Ceramics," *Phys. Stat. Sol.* (a), **47** [1] 139-44 (1978).
2. H. Schmalzried and C. Wagner, "Disorder Structure in Ternary Ionic Crystals *(in Ger.)*," *Z. Phys. Chem.*, **B31** 198-221 (1962).
3. H. Schmalzried, "Point Defect in Ternary Ionic Crystals,"; pp. 265-303 in Progress in Solid State Chemistry, Vol. 2, Edited by H. Reiss, North-Holland Publishing Co., Amsterdam, 1964.
4. F. A. Kröger, The Chemistry of Imperfect Crystals; 2nd ed., Chaps. 20 and 21, North-Holland Publishing Co., Amsterdam, 1974.
5. P. Abelard and J.F. Baumard, "Nonstoichiometry in Ternary Oxides. A New Graphical Representation of The Defect Configurations *(in Sweden)*," *Science of Ceramics*, **11** 143-48 (1981).
6. D. M. Smyth, "Thermodynamic Characterization of Ternary Compounds. I. The Case of Negligible Defect Association," *J. Solid State Chem.*, **16** [1-2] 73-81 (1976); "Thermodynamic Characterization of Ternary Compounds. II. The Case of Extensive Defect Association," *J. Solid State Chem.*, **20** [4] 359-64 (1977).
7. R. Waser, "Bulk Conductivity and Defect Chemistry of Acceptor-doped Strontium Titanate in the Quenched State," *J. Am. Ceram. Soc.*, **74** [8] 1934-40 (1991).
8. D. M. Smyth, The Defect Chemistry of Metal Oxides; Particularly Chap 14, Oxford University Press, New York, 2000.
9. M. Martin, Private communication.
10. H.-I. Yoo, C.-R. Song and D.-K. Lee, "$BaTiO_{3-\delta}$: Defect Structure, Electrical Conductivity, Chemical Diffusivity, Thermoelectric Power, and Oxygen Nonstoichiometry," *J. Electroceram.*, **8** 5-36 (2002).
11. H.-I. Yoo, S.-W. Lee and C.-E. Lee, "P-Type Partial Conductivity of Donor(La)-Doped $BaTiO_3$," *J. Electroceram.*, **10** 215-19 (2003).
12. C.-R. Song and H.-I. Yoo, "Chemical Diffusivity of $BaTiO_{3-\delta}$: I. Experimental Determination," *Solid State Ionics*, **120** [1-4] 141-53 (1999).
13. C.-R. Song and H.-I. Yoo, "Chemical Diffusivity of $BaTiO_{3-\delta}$: IV. Acceptor-doped Case," *J. Am. Ceram. Soc.*, **83** [4] 773-79 (2000).
14. D.E. Rase and R. Roy, "Phase Equilibria in the System $BaO\text{-}TiO_2$," *J. Am. Ceram. Soc.*, **38** [3] 102-13 (1955).
15. T. Negas, R.S. Roth, H.S. Parker and D. Minor, "Subsolidus Phase Relations in the Barium Titanate-titanium Dioxide System," *J. Solid State Chem.*, **9** [3] 297-307 (1974).
16. C.-R. Song and H.-I. Yoo, "Chemical Diffusivity of $BaTiO_{3-\delta}$: Defect-chemical Analysis," *Phys. Rev. B*, **61** [6] 3975-82 (2000).
17. H.-I. Yoo and K. D. Becker, "Effect of Hole-Trapping on Mass/Charge Transport Properties in Acceptor-doped $BaTiO_3$," *Phys. Chem. Chem. Phys.*, **7** 2068-73 (2005).
18. C. Wagner, "Determination of Small Deviations from the Ideal Stoichiometric Composition of Ionic Crystals and Other Binary Compounds," *Prog. Solid State Chem.*, **6** 1-15 (1971).
19. D.-K. Lee and H.-I. Yoo, "Oxygen Nonstoichiometry of undoped $BaTiO_{3-\delta}$," *Solid State Ionics*, **144** [1-2] 87-97 (2001).
20. D.-K. Lee, J.-I. Jeon, M.-H. Kim, W. Choi, and H.-I. Yoo, "Oxygen Nonstoichiometry (δ) of $TiO_{2-\delta}$ Revisited," *J. Solid State Chem.*, **178** [1] 185-93 (2005).
21. A.M.J.H. Seuter, "Defect Chemistry and Electrical Transport Properties of Barium Titanate," *Phil. Res. Rep. Suppl.*,

3 [1] 1-84 (1974).
22. H.-J. Hagemann and D. Hennings, "Reversible Weight Change of Acceptor-doped Barium Titanate," *J. Am. Ceram. Soc.*, **64** [10] 590-94 (1981).
23. G.V. Bois, N.A. Mikhailova, E.I. Prodavtsova and V.A. Yusova, "Partial Pressure of Oxygen and Oxygen Vacancies in Barium Titanate," *News. Acad. Sci. USSR, Inorg. Mat.*, **12** 1302 (1976).
24. R.J. Panlener and R.N. Blumenthal, "Titanium-rich Nonstoichiometric Barium Titanate. III. High-temperature Thermodynamic and X-ray Diffraction Measurements," *J. Am. Ceram. Soc.*, **54** [12] 610-13 (1971).
25. D. Hennings, "Defect Chemistry and Electrical Conductivity of Doped Barium Titanate Ceramics. Part III. Thermo-Gravimetric Investigations," *Philips Res. Rep.*, **31** [6] 516-25 (1976).
26. H.-I. Yoo, C.-R. Song, Y.-S. Lee and D.-K. Lee, "Surface Reaction Kinetics in Oxygen Nonstoichiometry Re-equilibration of $BaTiO_{3-\delta}$," *Solid State Ionics*, **160** [3-4] 381-87 (2003).
27. J. Crank, The Mathematics of Diffusion; 2nd ed., pp. 60-1, Clarendon Press, Oxford, U.K., 1975.
28. C. Wagner, "Theory of the Tarnishing Process *(in Ger.)*," *Z. Phys. Chem. B*, **21** 25-41 (1933).
29. W. Van Roosbroeck, "The Transport of Added Current Carriers in a Homogeneous Semiconductor," *Phys. Rev.*, **91** 282-89 (1953).
30. H.-I. Yoo and C.-E. Lee, "Two-Fold Diffusion Kinetics of Oxygen Re-equilibration in Donor-doped $BaTiO_3$," *J. Am. Ceram. Soc.*, **88** [3] 617-23 (2005).
31. J. Nowotny and M. Rekas, "Defect Structure, Electrical Properties and Transport in Barium Titanate. VII. Chemical Diffusion in Nb-doped $BaTiO_3$," *Ceram. Int.*, **20** [4] 265-75 (1994).
32. R. Wernicke, "Defect Chemistry and Electrical Conductivity of Doped Barium Titanate Ceramics. Part IV. The Kinetics of Equilibrium Restoration in Barium Titanate Ceramics," *Philips Res. Rep.*, **31** [6] 526-43 (1976).
33. G. V. Lewis and C. R. A. Catlow, "Computer Modeling of Barium Titanate," *Radiation Effects*, **73** [1-4] 307-14 (1983).
34. D.-K. Lee and H.-I. Yoo, "Unusual Oxygen Re-equilibration Kinetics of $TiO_{2-\delta}$," *Solid State Ionics*, **177** [1-2] 1-9 (2006).